MOMENTUM ACCUMULATION DUE TO SOLAR RADIATION TORQUE, AND REACTION WHEEL SIZING, WITH CONFIGURATION OPTIMIZATION

Hari B. Hablani†
Rockwell International, Space Systems Division, Seal Beach, CA 90740

Abstract

This paper has a two-fold objective: determination of yearly momentum accumulation due to solar radiation pressure, and optimum reaction wheel sizing. The first objective is confronted while determining propellant consumption by the attitude control system over a spacecraft's lifetime. This, however, cannot be obtained from the daily momentum accumulation and treating that constant throughout the year, because the orientation of the solar arrays relative to the spacecraft changes over a wide range in a year, particularly if the spacecraft has two arrays, one normal and the other off-normal to different extent at different times to the sun rays . The paper therefore first develops commands for the arrays for tracking the sun, the arrays articulated to earth-pointing spacecraft with two rotational degrees of freedom and spacecraft in an arbitrary circular orbit. After developing expressions for solar radiation torque due to one or both arrays, arranged symmetrically or asymmetrically relative to the spacecraft bus, momentum accumulation over an orbit and then over a year are determined. The remainder of the paper is concerned with designing reaction wheel configurations. Four-, six-, and three-wheel configurations are considered, and for given torque and momentum requirements, their cant angles with the roll/yaw plane are optimized for minimum power consumption. Finally, their momentum and torque capacities are determined for one-wheel failure scenario, and six configurations are compared and contrasted.

1. Introduction

This paper is concerned with: a) determination of momentum accumulation due to solar radiation torque acting on an earth-observing spacecraft with sun-pointing solar arrays, and b) reaction wheel sizing and its pyramid configuration optimization for maximum momentum storage and minimum power consumption. These topics are classical; yet it seems there is no single reference in the published literature that treats this subject with sufficient comprehensiveness so that a control engineer, confronting this task, could accurately size the reaction wheels, select a wheel configuration, and estimate yearly propellant consumption for momentum dumping, all without extensive or expensive computer simulation. This paper, hopefully, fulfills that need. The contents of the paper and related previous contributions known to this author are summarized below.

Solar arrays' influence on spacecraft configuration, attitude control system, and mission operation is so far-reaching that a brief elaboration of this topic appears in order. For an earth-pointing three-axis stabilized spacecraft rotating once per orbit about the orbit normal, an attached solar array must at least have one relative rotational degree of freedom about the orbit normal so that the array can be held inertially fixed and sun-pointing. Although economical, this arrangement becomes inadequate if the spacecraft's life span is more than several (say, six) months, because in this duration the earth moves around the sun in the ecliptic plane so much that the sun-rays deviate significantly away from the array normal and therefore a considerable power loss begins to occur. Consequently, for spacecraft with one year or longer life span, the solar array is accorded a second degree of freedom in the form of spacecraft yaw rotation. If the spacecraft at hand has only one solar array, this yaw rotation is of 180 degrees and may take place once in six months when the off-normality between the sun-rays and the array on one side of the orbit plane exceeds limits. The 180-degree rotation takes the solar array to the other side of the orbit plane where the off-normality in the following six months will be smaller. Although to minimize cost and to gain simplicity, there are many spacecraft with one solar array (TOPEX for example), this configuration is asymmetric and might generate significant disturbance torques on the spacecraft arising from solar radiation pressure, gravity gradient, atmospheric drag, and thermal shocks at each sun-rise and sun-set; savings are therefore somewhat offset by stronger control torque requirements. To eliminate this asymmetry and/or to generate enough power for on-orbit needs, two solar arrays, one on each side of the orbit normal, are sometimes employed. Then, instead of once in six months, a yaw rotation from zero to 2π or from $-\pi/2$ to $+\pi/2$ takes place as continuously as one about the orbit normal. The corresponding sun-tracking commands were derived by McElvain (1961)[1] and Kalweit (1983)[2]. GPS satellites have opted for this approach. Although TOPEX satellite has one solar array, it also employs continuous yaw rotation instead of 180° yaw rotation. Some missions are not interfered with by these persistent yaw rotations, but others are. For these latter situations, Kalweit[2] has determined best-fit minimum-power-loss, average yaw angles, constant over each half orbit. Nonetheless, persistent yaw rotation of a spacecraft is cumbersome because the torque and momentum capacity of the reaction wheels, usually employed for attitude control, must now accommodate the yaw rotation. A superior alternative appears to be, at least on the basis of technical merits if not cost, to bestow each array with two rotational degrees of freedom relative to the spacecraft, one about the orbit normal and the other about an axis in the orbit plane. Such is the spacecraft configuration considered in this paper; that is, a spacecraft with two solar arrays, arranged symmetrically on each side of the orbit normal and each array having two articulation degrees of freedom. Section 2 of the paper furnishes sun-tracking commands about the two just-mentioned axes. Explicit relationship is furnished between the so-called beta angle (also called flap angle) of the array and parameters such as earth's position in the ecliptic plane, the angle between the ecliptic and the equator planes, inclination of the spacecraft orbit, and its ascending node angle.

†*Senior Member AIAA, Senior Engineering Specialist; Guidance, Control, and Navigation Group*

Turning our attention to solar radiation torque on a space vehicle, this arises from arrays as well as the vehicle bus. Moreover, of the two arrays, one may be normal to the sun while the other may be off-normal (thermal requirements may dictate so), and the bus and the arrays may cast shadow on each other at different times, changing the lit area, center of pressure, and moment arm from the vehicle mass center to the pressure center; see an example of shadowing in Evans (1964)[3]. These complex effects are formulated and illustrated in Section 3. For typical spacecraft however, the torque contribution of the bus and the shadow effects are secondary; so by ignoring them, simple radiation torque expressions for arrays normal as well as off-normal to the sun are obtained which are used in Section 4 to determine secular and cyclic momentum accumulation in the roll-yaw plane and about the pitch axis. Because of significant variation in the array's flap angle over a year, the corresponding momentum accumulation over each orbit changes considerably, particularly if the array is positioned off-normal to the sun. A simple expression of annual, secular momentum accumulation is therefore developed and illustrated in Section 4, and its dependence on the orbit inclination is investigated. From this result, yearly propellant consumption for momentum dumping is determined easily. DeBra and Cannon (1961)[4] have also performed preliminary analysis along these lines.

Section 5 of the paper is concerned with sizing reaction wheels and optimizing their pyramid configuration, keeping cost and redundancy in mind. Four-, six-, and three-wheel configurations with and without one wheel failure are considered. Optimum cant angles for these pyramid configurations for minimum power consumption and for given ratios between the roll, pitch, and yaw torque requirements are determined. Simple relationships are developed relating momentum or torque requirements about spacecraft axes to those about the wheel axes for all configurations with and without one wheel failure. These relationships then provide the required momentum and torque capacities of the wheels. The paper is finally concluded in Section 6.

2. Commands for Sun-Tracking

Coordinate Transformations

In order to express sun-ray direction from the sun to the Earth in terms of solar arrays' frames, and to develop pointing commands for the arrays for tracking the sun,the following angles, all anticlockwise positive unless stated otherwise, are introduced. The angle ν, measured from the the first day of *autumn* (September 23), denotes the earth's rotation around the sun in the ecliptic plane. The *clockwise* positive angle λ (= 23.44 degrees) about the Vernal Equinox is the angle between the ecliptic and the equatorial plane. The angle Ω_N and i are, respectively, the usual ascending node angle of the spacecraft orbit in the equatorial plane and the orbit inclination angle from the equatorial plane. In this paper we will be concerned exclusively with circular spacecraft orbit. The local-vertical-local-horizontal (LVLH) frame $\mathcal{F}^c$: $X_c\ Y_c\ Z_c$ at any point in the orbit locates the spacecraft mass center with X_c along the velocity vector of the spacecraft, Z_c along the local vertical from spacecraft to the earth, and Y_c opposite to the orbit normal. To maintain the earth-pointing attitude, the spacecraft rotates clockwise about Y_c-axis at the rate $-\omega_0$ (ω_0 thus is a positive quantity and it equals the orbit rate of the spacecraft). The frame $\mathcal{F}^c$ is the standard roll, pitch, yaw frame of a spacecraft with these three attitude angles zero. When the angles are nonzero, the spacecraft frame is denoted $\mathcal{F}^0$: $X_0\ Y_0\ Z_0$, as shown in Fig. 1. In this paper however, we assume that the spacecraft is controlled perfectly, and it always maintains its ideal LVLH orientation.

We now define the orientation of the solar arrays relative to the frame $\mathcal{F}^c$ or, equivalently, $\mathcal{F}^0$. As stated in the Introduction and portrayed in Fig. 1, the two arrays turn relative to the spacecraft at the two-degree-of-freedom hinges O_1 and O_2. Considering +y-array first, its relative rotation is measured from the frame $X_{10}\ Y_{10}\ Z_{10}$ which is parallel to the spacecraft frame $\mathcal{F}^0$. In order to track the sun, the first rotation of the array is θ_{1y} about the longitudinal axis y_{10}; this rotation annuls the clockwise rotation $\omega_0 t$ of the earth-pointing spacecraft measured from the ascending node line. The second rotation (often called beta angle), denoted here θ_{1z}, takes place about the once-displaced Z_{10}-axis. We thus arrive at the array-fixed frame $\mathcal{F}^1$: $X_1\ Y_1\ Z_1$, with the array in the Y_1Z_1 plane and its outward normal along X_1. Note that when the array is normal to the sun, the sun vector $\underline{S}$ from the sun to the earth is opposite to the array normal X_1. The transformation between the frame $\mathcal{F}^0$ and the array frame $\mathcal{F}^1$ for the sequence θ_{1y}, θ_{1z} is

$$\begin{bmatrix} X_0 \\ Y_0 \\ Z_0 \end{bmatrix} = \begin{bmatrix} c\theta_{1y}\,c\theta_{1z} & -c\theta_{1y}\,s\theta_{1z} & s\theta_{1y} \\ s\theta_{1z} & c\theta_{1z} & 0 \\ -s\theta_{1y}\,c\theta_{1z} & s\theta_{1y}\,s\theta_{1z} & c\theta_{1y} \end{bmatrix} \begin{bmatrix} X_1 \\ Y_1 \\ Z_1 \end{bmatrix} \tag{1}$$

where $c(\cdot) = \cos(\cdot)$ and $s(\cdot) = \sin(\cdot)$. The initial orientation of the $-y$-array is the same as that of the $+y$-array, and the rotations of the $-y$ array are conveniently measured relative to the frame $X_{20}Y_{20}Z_{20}$ with Y_{20} opposite to Y_0 and Z_{20} opposite to Z_0. The frame $X_{20}Y_{20}Z_{20}$ is selected such that the solar cell face of both arrays are on the same side. The first rotation θ_{2y} about the Y_{20}-axis (Fig. 1) nullifies the orbit rotation, and the rotation θ_{2z} about the edge Z_2 brings the array to the desired normal orientation relative to the sun. The transformation matrix from the spacecraft frame $\mathcal{F}^0$ to the array-fixed frame $\mathcal{F}^2$: $X_2Y_2Z_2$ is

$$\begin{bmatrix} X_0 \\ Y_0 \\ Z_0 \end{bmatrix} = \begin{bmatrix} c\theta_{2z}\,c\theta_{2y} & -s\theta_{2z}\,c\theta_{2y} & s\theta_{2y} \\ -s\theta_{2z} & -c\theta_{2z} & 0 \\ c\theta_{2z}\,s\theta_{2y} & -s\theta_{2z}\,s\theta_{2y} & -c\theta_{2y} \end{bmatrix} \begin{bmatrix} X_2 \\ Y_2 \\ Z_2 \end{bmatrix} \tag{2}$$

Commands For Sun-Tracking

Because the solar arrays are hinged to the spacecraft, it is helpful to express the unit vector $\underline{S}$ from the Sun to the Earth in the spacecraft frame $\mathcal{F}^0$, or equivalently, in the orbit frame $\mathcal{F}^c$. Let S_{c1}, S_{c2}, and S_{c3} be the components of $\underline{S}$ in $\mathcal{F}^c$. Then, using coordinate transformations involving the angles ν, λ, Ω_N, i, and $\omega_0 t$, defined above, these components are found to be

$$\begin{aligned} S_{c1} &= c\omega_0 t\,\{ci(-s\Omega_N c\nu + c\Omega_N c\lambda s\nu) + sis\lambda s\nu\} \\ &\quad -s\omega_0 t(c\Omega_N c\nu + s\Omega_N\, c\lambda s\nu) \\ S_{c2} &= si(-s\Omega_N c\nu + c\Omega_N c\lambda s\nu) - cis\lambda s\nu \\ S_{c3} &= -s\omega_0 t\,\{ci(-s\Omega_N c\nu + c\Omega_N c\lambda s\nu) + sis\lambda s\nu\} \\ &\quad -c\omega_0 t(c\Omega_N c\nu + s\Omega_N\, c\lambda s\nu) \end{aligned} \tag{3}$$

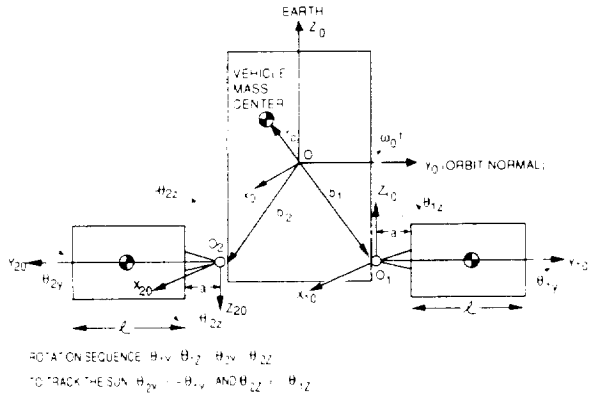

Fig. 1. A Spacecraft with +Y and -Y Arrays, their Frames, and Articulation Degrees of Freedom

+Y-Array Commands

Because the first rotation θ_{1y} about the longitudinal axis y_{10} annuls the once-per-orbit rotation of the earth-pointing spacecraft, it may be clear that, ideally,

$$\theta_{1y}(t) = \omega_0 t + \theta_{10} \tag{4}$$

where θ_{10} is $\theta_{1y}(t=0)$. Note that $\theta_{1y}(t)$ is anticlockwise positive, whereas the negative sign of $\omega_0 t$ has already been accounted for in (3), so $\omega_0 t$ in Eq. (4) is positive: $\omega_0 t \geq 0$. To determine θ_{10} and the second rotation θ_{1z}, we observe that when the array is normal to the sun, the incoming sun vector $\underline{S}$ is opposite to the outgoing array normal X_1:

$$\underline{S}^{\mathcal{F}1} = [\, X_1 \;\; Y_1 \;\; Z_1 \,]^T = [\, -1 \;\; 0 \;\; 0 \,]^T \tag{5}$$

where the superscript T means the transpose of the column vector. Substituting Eq. (5) in Eq. (1) the sun-ray vector $\underline{S}$ in the LVLH frame is found to be

$$\begin{bmatrix} S_{c1} \\ S_{c2} \\ S_{c3} \end{bmatrix}^{\mathcal{F}0} = \begin{bmatrix} -c\theta_{1y}\, c\theta_{1z} \\ -s\theta_{1z} \\ s\theta_{1y}\, c\theta_{1z} \end{bmatrix} \tag{6}$$

The unknown initial angle θ_{10} is determined by substituting Eq. (4) in Eq. (6), yielding:

$$\theta_{10} = \tan^{-1} \frac{-[\, c\Omega_N\, cv + s\Omega_N\, c\lambda\, sv]}{-[\, ci\,(-s\Omega_N\, cv + c\Omega_N\, c\lambda\, sv) + si\, s\lambda\, sv\,]} \tag{7}$$

where the negative signs in the numerator and denominator are retained so as to arrive at a unique value of θ_{10} within the range $-\pi \leq \theta_{10} \leq \pi$; this will ensure that the solar cell face of the array looks at the sun. The array's inclination angle θ_{1Z} is obtained from the second components of Eqs. (3) and (6):

$$\theta_{1Z} = \sin^{-1}(si\,(s\Omega_N\, cv - c\Omega_N\, c\lambda\, sv) + ci\, s\lambda\, sv] \tag{8}$$

Eq. (8) indicates that, as the earth rotates around the sun ($0 \leq v \leq 2\pi$), the angle θ_{1z} varies sinusoidally with a certain amplitude; this is illustrated below in three examples.

Example 1: $\Omega_N = 0$, $v = \pi/2$

The correctness of Eq. (7) and Eq. (8) can be illustrated by considering $v = \pi/2$ and $\Omega_N = 0°$ for which

$$\theta_{10} = \tan^{-1}\, 0 / [\, -c\,(\lambda - i\,)\,] \;\; = \pi \tag{9a}$$

$$\theta_{1z} = \lambda - i \tag{9b}$$

If we further assume that the satellite orbit lies in the ecliptic plane, which means the orbit inclination i equals λ, we will have $\theta_{1Z} = 0$. In Eq. (9a), the choice $\theta_{10} = \pi$ and not zero is selected to ensure that the solar cell face of the array, not its back side, is towards the sun. Moreover, Eq. (9a) and $\theta_{1z} = 0$ together imply that in order to be normal to the sun rays at $t = 0$, the array must be in the plane $Y_c\, Z_c$. Physically, the conclusion $\theta_{10} = \pm\pi$ and $\theta_{1z} = 0$ is seen to be valid in Fig. 2 for the parameters $v = \pi/2$, $\Omega_N = 0$, and $i = \lambda$ at $t = 0$.

Example 2: $\Omega_N = 0$, and arbitrary v

For $\Omega_N = 0$, Eq. (7) and Eq. (8) yield

$$\theta_{10} = \tan^{-1} \frac{-cv}{-c\,(\lambda\text{-}i)\, sv}, \quad \theta_{1z} = \sin^{-1}[\, \sin v \sin(\lambda\text{-}i)\,] \tag{10a,b}$$

Eq. (10b) states that, inasmuch as $(\lambda - i)$ is fixed, the angle θ_{1z} will change periodically as the earth moves around the sun in one year, $0 \leq v \leq 2\pi$; the extremes of θ_{1z} will be $(\lambda - i)$ when $v = \pi/2$, and $(i - \lambda)$ when $v = 3\pi/2$. This is illustrated in Fig. 3 for $i = 28.5°$ and $43.5°$. Now considering the satellite orbit in the ecliptic plane ($\lambda = i$), Eqs. (10) simplify and, consistent with Example 1, furnish

$$\theta_{10} = -\pi/2 - v \tag{11a}$$

$$\theta_{1y}(t) = \omega_0 t - (\pi/2 + v) \tag{11b}$$

For $v = 0$, +y array's rotation $\theta_{10} = -\pi/2$ about the axis Y_c, measured from its datum orientation in the $Y_c Z_c$ plane, is illustrated in Fig. 2. Also, for $\Omega_N = 0$ and $i = 28.5°$ the linear relationship (11a) is seen to be true in Fig. 3.

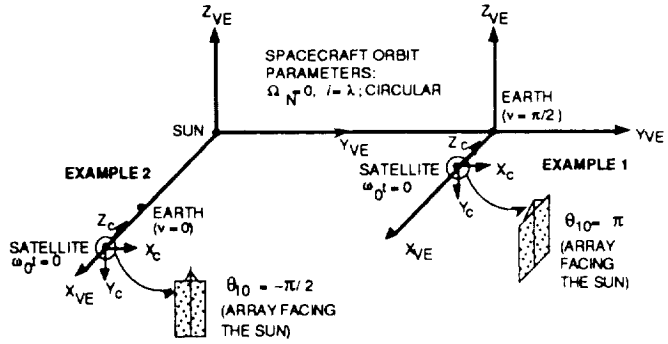

Fig. 2. +y Solar Array Orientations at t=0 for Examples 1 and 2 (VE = Vernal Equinox)

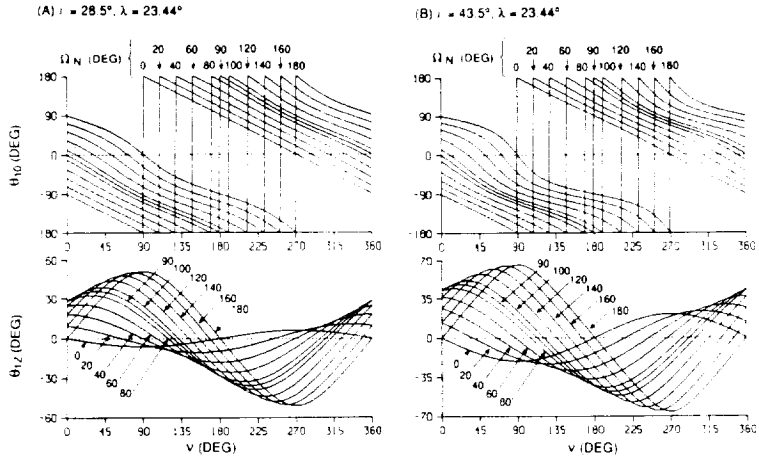

Fig. 3. Initial Angle θ_{10} about the pitch axis y_0 and inclination angle θ_{1z} about the short edge Z_1-axis of +y array versus angle ν

Table 1. Extrema of the tilt angle θ_{1z}

Earth's Position in the Ecliptic Plane (ν,deg)	Ascending Node Angle of the Spacecraft's Orbit (Ω_N, deg)	Extreme Value of θ_{1z}
90°	0 °	λ–i
90°	180 °	λ+i
-90° (or 270°)	0 °	i–λ
-90° (or 270°)	180 °	–λ–i

Example 3: Arbitrary Ω_N and ν

Fig. 3 illustrates the variation of θ_{10} and θ_{1Z} as a function of the earth's position in the ecliptic plane ($0 \le \nu \le 2\pi$) for i = 28.5° and 43.5° and eleven values of the ascending node angle Ω_N. The apparent discontinuities in θ_{10} curves at $\pm\pi$ are inconsequential because the angle θ_{10} has a range of 2π and $+\pi = -\pi$. Furthermore, from Eq. (8), we infer that

$$\text{for } \Omega_N = \pi: \ \theta_{1Z} = \sin^{-1}[\, s(\lambda+i)\, s\nu \,] \qquad (12)$$

which is a counterpart of Eq. (10b) in Example 2. Clearly, the extremes of θ_{1Z} are

$$\theta_{1z} = \begin{cases} \lambda+i \ @ \ \nu = \pi/2 \\ -(\lambda+i) \ @ \ \nu = 3\pi/2 \end{cases} \qquad (13)$$

These, as well as the sinusoidal variation of the angle θ_{1Z} versus ν, are illustrated in Fig. 3. Also, see Table 1.

–Y Array Commands

Regarding the –y-array, because the angles θ_{2y} and θ_{2z} are defined about the axes Y_{20} and Z_{20} which are respectively opposite to the +y-array axes Y_{10} and Z_{10}, it is clear that for keeping the array normal to the sun-rays

$$\theta_{2y} = -\theta_{1y} \qquad (14a)$$
$$\theta_{2z} = -\theta_{1z} \qquad (14b)$$

Recalling Eq. (4), the desired $\theta_{2y}(t)$ will therefore be

$$\theta_{2y}(t) = -\omega_0 t - \theta_{10} \qquad (15)$$

It is instructive to compare the commands developed above with those developed by McElvain[1] and Kalweit[2].

3. Solar Radiation Torque

Radiation Torque on a Solar Array

For momentum accumulation study, the radiation torque $\underline{g}$ at the spacecraft mass center is required. Referring to Fig. 1, let $\underline{b}_j$ (j = 1,2) be the vector from the reference origin O to the solar array hinge O_j (j = 1,2), and $\underline{\rho}_{pj}$ (j = 1,2) the vector from the hinge O_j to the pressure (or geometric) center of the array. Additionally, let $\underline{r}_c$ be the vector from the reference origin to the vehicle mass center. Denote the moment arm vector of the solar radiation force on the j-array as $\underline{c}_{pj}$. Then,

$$\underline{c}_{pj} \triangleq -\underline{r}_c + \underline{b}_j + \underline{C}_{0j}\, \underline{\rho}_{pj} \qquad (j = 1,2) \qquad (16)$$

where $\underline{C}_{0j}$ is the transformation matrix defined by Eq. (1) and Eq. (2) for j=1.2. Following Reference 5, Section 8.3, the radiation torque experienced by a spacecraft about its mass center owing to the sun rays off-normal to the jth-array, is

$$\underline{g}_j = pA_j c\alpha_j \underline{c}_{pj}^{\times} [\, (\sigma_a + \sigma_{rd})\, \underline{S} + 2\,(\sigma_{rd}/3 + \sigma_{rs}\, c\alpha_j)\, \underline{n}_{Aj} \,] \quad (j=1,2) \qquad (17)$$

where p denotes the radiation pressure on a totally absorbing normal surface, A_j is the array's area, $c\alpha_j = \cos\alpha_j$ and α_j is the angle between the inward normal unit vector $\underline{n}_{A_j}$ and the sun vector $\underline{S}$, σ_a is the absorptivity coefficient of the surface under consideration, σ_{rd} is the diffused reflectivity coefficient, and σ_{rs} the specular reflectivity coefficient. The notation × in Eq. (17) transforms a column vector to a 3x3 skew-symmetric matrix, as defined by Eq. (13), Section B.2, Reference 5.

Array Normal to the Sun

When the sun rays are normal to the j^{th} array, $c\alpha_j = 0$, and $\underline{n}_{Aj} = \underline{S}$ and Eq. (17) simplifies to

$$\underline{g}_j = pA_j \sigma_A \underline{\rho}_{pj}^{\times} \underline{S} \tag{18}$$

where

$$\sigma_A = 1 + \sigma_{rs} + 2\sigma_{rd}/3 \tag{19}$$

The three components of the radiation torque, Eq. (18), on the spacecraft in an arbitrary orbit, with the array normal to the sun, will now be shown explicitly. For concreteness, we assume that the spacecraft mission is such that the power and thermal requirements allow the +y-array to be normal to the sun. To express the vector $\underline{\rho}_{p1}$ component-wise, note that the length of the A-frame along the pitch axis is 'a' (Fig. 1), and the rotation θ_{1z} takes place about the Z_1-axis of the array without involving the A-frame. Because in the $X_1Y_1Z_1$ frame, the pressure center of the array is at a distance $\ell/2$ along the y_1-axis from the transverse edge of the array (Fig. 1), the vector $\underline{C}_{01}\,\underline{\rho}_{p1}$ in Eq. (16) can be calculated easily using Eq. (1). Furthermore, we assume that when the arrays are in the y_0z_0 plane ($\theta_{1z} = 0 = \theta_{2z}$), the vectors $\underline{r}_c$ and $\underline{b}_1$ are in that plane (Fig. 1). Therefore, in the LVLH frame $\mathcal{F}^c$:

$$-\underline{r}_c + \underline{b}_1 = [\ 0 \qquad -r_{cy}+b_{1y} \qquad -r_{cz}+b_{1z}\ ]^T \tag{20}$$

The vector $\underline{\rho}_{p1}$, Eq. (16), will therefore be

$$\underline{\rho}_{p1} = \begin{bmatrix} -b\, s\theta_{1z}\, c\theta_{1y} \\ -r_{cy} + b_{1y} + a + b\, c\theta_{1z} \\ -r_{cz} + b_{1z} \qquad +b\, s\theta_{1z} s\theta_{1y} \end{bmatrix}, \quad b \triangleq \ell/2 \tag{21}$$

For analytical convenience, define

$$b_{1y}^{\oplus} = -r_{cy} + b_{1y} + a \qquad b_{1z}^{\oplus} = -r_{cz} + b_{1z} \tag{22}$$

Using (21), (22)in Eq. (18) the following components of the torque $\underline{g}_1$ in the LVLH frame are obtained:

$$\underline{g}_1 = pA_1 \sigma_A \begin{bmatrix} b_{1z}^{\oplus} s\theta_{1z} + (b + b_{1y}^{\oplus} c\theta_{1z})\, s\theta_{1y} \\ -b_{1z}^{\oplus} c\theta_{1z}\, c\theta_{1y} \\ (b + b_{1y}^{\oplus} c\theta_{1z})\, c\theta_{1y} \end{bmatrix}^{\mathcal{F}_c} \tag{23}$$

While the angle $\theta_{1y}(t)$ varies linearly at the rate ω_o, changing by 2π over one orbital period, the angle θ_{1z} is virtually constant in that period. Eq. (23) therefore indicates that, in the LVLH frame, the roll (x-) torque comprises a constant and a cyclic torque, the pitch and yaw torques are cyclic, and the cyclic yaw torque is in quadrature with the cyclic component of the roll torque. (Also, see Ref. 4.)

–Y-Array Off-Normal To The Sun

When the spacecraft at hand has two arrays, power and thermal requirements might dictate one array to be normal to the sun rays and the other array off-normal. Fig. 4 depicts one such posture for the spacecraft in Fig. 1, with +Y-array normal and –Y-array off-normal.

To keep the mass center of the –y-array on the rotational axis y_0, the A-frame is turned about the z_2-axis by an angle $\theta_{2z,a}$ (a negative $\theta_{2z,a}$ is shown in Fig. 4); also, the array's normal-to-the-sun orientation angle is denoted θ_{2z}, whereas the off-normal orientation angle is denoted θ_{2z}'. Under these circumstances, the transformation matrix $\underline{C}_{02}$, defined by Eq. (2), is altered to $\underline{C}_{02,A}$ for the A-frame replacing θ_{2z} with $\theta_{2z,a}$, and to $\underline{C}_{02}'$ for the –y-array substituting θ_{2z}' for θ_{2z}. Thus the pressure center vector $\underline{C}_{02}\,\underline{\rho}_{p2}$ in Eq. (16) is revised to

$$\underline{C}_{02}\,\underline{\rho}_{p2} = = a \begin{bmatrix} -s\theta_{2z,a}\, c\theta_{2y} \\ -c\theta_{2z,a} \\ -s\theta_{2z,a}\, s\theta_{2y} \end{bmatrix} + b \begin{bmatrix} -s\theta_{2z}'\, c\theta_{2y} \\ -c\theta_{2z}' \\ -s\theta_{2z}'\, s\theta_{2y} \end{bmatrix} \tag{24}$$

To evaluate the torque $\underline{g}_j$ (j=2), we note that the vector $-\underline{r}_c + \underline{b}_2$ for the –y-array in the frame $\mathcal{F}^c$ is, following Eq. (20)

$$-\underline{r}_c + \underline{b}_2 = [\ 0 \qquad -r_{cy} + b_{2y} \qquad -r_{cz} + b_{2z}\ ]^T \tag{25}$$

where, to symmetrize the mass distribution

$$b_{2y} = -b_{1y} \qquad b_{2z} = b_{1z} \tag{26}$$

Using the equation $\theta_{2y} = -\theta_{1y}$ and Eqs. (24), (25), and (26), the vector $\underline{\rho}_{pj}$ (j = 2), Eq. (16), is found to be

$$\underline{\rho}_{p2} = \begin{bmatrix} -b_s\, c\theta_{1y} \\ -r_{cy} - b_{1y} - b_c \\ -r_{cz} + b_{1z} + b_s\, s\theta_{1y} \end{bmatrix}^{\mathcal{F}^c} = \begin{bmatrix} \rho_{p2x} \\ \rho_{p2y} \\ \rho_{p2z} \end{bmatrix}^{\mathcal{F}^c} \tag{27}$$

where the lengths b_c and b_s are defined as

$$\begin{aligned} b_c &= a\, c\theta_{2z,a} + b\, c\theta_{2z}' \\ b_s &= a\, s\theta_{2z,a} + b\, s\theta_{2z}' \end{aligned} \tag{28}$$

The vector $\underline{S}$ and the inward normal $\underline{n}_A$ for the –y-array in the off-normal frame $\mathcal{F}^{2A}$: $X_{2A}\, Y_{2A}\, Z_{2A}$ (Fig. 4) are

$$\underline{S}^{\mathcal{F}^{2A}} = [-c\delta_{2z} \quad -s\delta_{2z} \quad 0\ ]^T, \quad \underline{n}_A^{\mathcal{F}^{2A}} = [\ -1 \quad 0 \quad 0\ ]^T \tag{29}$$

where δ_{2z} is the off-normal angle, defined by

$$\delta_{2z} = \theta_{2z} - \theta_{2z}' \tag{30}$$

and equal to the angle α_2 between the vectors $\underline{S}$ and $\underline{n}_A$ for the array. Therefore the vector [•] in (17) the spacecraft frame is found to be

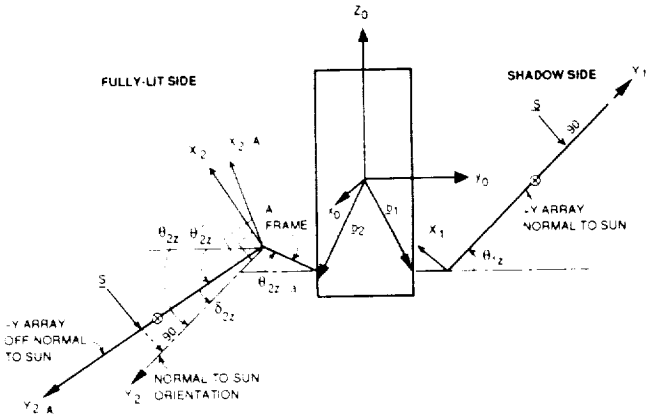

Fig. 4. A Spacecraft With +Y Array Normal to the Sun and -Y Array Off-Normal

$$[\,(\sigma_a + \sigma_{rd})\,\underline{S} + 2\,(\sigma_{rd}/3 + \sigma_{rs}\,c\alpha_2)\,\underline{n}_A\,]^{\mathcal{F}^0} = [\,-\sigma_{cx}\,c\theta_{2y} \quad \sigma_{cy} \quad -\sigma_{cx}\,s\theta_{2y}\,]^T \tag{31}$$

where

$$\begin{aligned}\sigma_{cx} &= \sigma_{x2}\,c\theta_{2z}' - \sigma_{y2}\,s\theta_{2z}'\\ \sigma_{cy} &= \sigma_{x2}\,s\theta_{2z}' + \sigma_{y2}\,c\theta_{2z}'\\ \sigma_{x2} &= (1+\sigma_{rs})\,c\delta_{2z} + 2\sigma_{rd}/3\\ \sigma_{y2} &= (1-\sigma_{rs})\,s\delta_{2z}\end{aligned} \tag{32}$$

Using the vector $\underline{\varsigma}_{p2}$ in Eq. (27) and the vector Eq. (31) the torque $\underline{g}_2$ is found to be

$$\underline{g}_2^{\mathcal{F}^c} = pA_2\,c\delta_{2z}$$

$$\begin{bmatrix} -(-r_{cz}+b_{1z})\,\sigma_{cy} - \{b_s\,\sigma_{cy} + (r_{cy}+b_{1y}+b_c)\,\sigma_{cx}\}s\theta_{1y} \\ -(-r_{cz}+b_{1z}) \quad \sigma_{cx}\}c\theta_{1y} \\ -\{b_s\,\sigma_{cy} + (r_{cy}+b_{1y}+b_c)\,\sigma_{cx}\}c\theta_{1y} \end{bmatrix} \tag{33}$$

which exhibits the same attributes as those exhibited by $\underline{g}_1$ in Eq. (23).

Example 1: Off-Normal Angle $\delta_{2z} = 0$ and A-Frame Angle $\theta_{2z,a} = 0$

In this circumstance, the +y- and -y-array become parallel because now $\theta_{2z}' = -\theta_{1z}$, and the torque $\underline{g}_2^{Fc}$, Eq. (33), simplifies to

$$\underline{g}_2^{\mathcal{F}^c} = pA_2\,\sigma_A \begin{bmatrix} b_{2z}^{\oplus}\,s\theta_{1z} + (-b + b_{2y}^{\oplus}\,c\theta_{1z})\,s\theta_{1y} \\ -b_{2z}^{\oplus}\,c\theta_{1z}\,c\theta_{1y} \\ (-b + b_{2y}^{\oplus}\,c\theta_{1z})\,c\theta_{1y} \end{bmatrix} \tag{34}$$

where

$$b_{2y}^{\oplus} = -r_{cy} - b_{1y} - a \qquad b_{2z}^{\oplus} = b_{1z}^{\oplus} \tag{35}$$

Example 2: Both Arrays Normal to the Sun: Resultant Torque

Adding Eq. (34) to Eq. (23), and assuming that the arrays are identical in geometry as well as in optical surface properties so that $A_s = A_1 = A_2$, the resultant torque $\underline{g}$ equal to $\underline{g}_1 + \underline{g}_2$) is found to be

$$\underline{g}^{\mathcal{F}^c} = 2pA_s\,\sigma_A \begin{bmatrix} (-r_{cz}+b_{1z})\,s\theta_{1z} - r_{cy}\;c\theta_{1z}\,s\theta_{1y} \\ (r_{cz}-b_{1z})\,c\theta_{1z}\,c\theta_{1y} \\ -r_{cy}\,c\theta_{1z}\,c\theta_{1y} \end{bmatrix} \tag{36}$$

Mass asymmetries in the spacecraft generate the components r_{cy} and r_{cz}; how each component contributes to the radiation torque on the spacecraft is seen clearly in Eq. (36). We also observe that, because the two arrays are parallel and geometrically identical, the A-frame length a and the array's half-length b do not contribute to the total torque, only the hinge location referenced from the vehicle mass center matters.

Example 3: +y-Array Normal and -y-Array Off-Normal: Resultant Torque

The resultant torque $\underline{g}^{\mathcal{F}^c}$ is now obtained by adding Eq. (23) with Eq. (33). To build a simple expression for $\underline{g}^{\mathcal{F}^c}$, we observe that, in the $\mathcal{F}^c$ frame, ignoring the variation in the angle θ_{1z} over one orbit period, the constant part g_c of the x-torque (roll torque) is found to be

$$g_c \triangleq pA_s\,b_{1z}^{\oplus}\,[\sigma_A\,s\theta_{1z} - \sigma_{cy}\,c\delta_{2z}) \tag{37a}$$

and the amplitude g_a of the sinusoidally varying part $g_a\,s\theta_{1y}$ of the x-torque is

$$g_a \triangleq pA_s\,[\sigma_A\,(b + b_{1y}^{\oplus}\,c\theta_{1z}) - c\delta_{2z}\,\{b_s\,\sigma_{cy} + (r_{cy}+b_{1y}+b_c)\,\sigma_{cx}\}\,] \tag{37b}$$

The z-component (yaw torque) has no constant part, and its sinusoidal variation is in quadrature with the roll component. Lastly, the y-component (pitch torque) also varies sinusoidally, with its amplitude g_b equal to

$$g_b = -pA_s\,b_{1z}^{\oplus}\,[\sigma_A\,c\theta_{1z} + \sigma_{cx}\,c\delta_{2z}] \tag{37c}$$

Thus, the total radiation torque $\underline{g}^{\mathcal{F}^c}$ acting on the spacecraft at its mass center, in the spacecraft frame, is

$$\underline{g}^{\mathcal{F}^c} = \begin{bmatrix} g_c + g_a\,s\theta_{1y} \\ g_b\,c\theta_{1y} \\ g_a\,c\theta_{1y} \end{bmatrix} \tag{37d}$$

The constant roll torque g_c in the rotating frame $\mathcal{F}^c$ becomes a periodic torque in the orbit plane in a non-rotating frame; conversely, the periodic roll-yaw torque in $\mathcal{F}^c$ becomes a constant torque in the orbit plane in an inertial frame.

Meanwhile, the periodic pitch torque remains periodic even in a non-rotating frame because the rotation $\omega_0 t$ takes place about the pitch axis.

Radiation Torque on Spacecraft Bus

Usually the surface area of spacecraft bus is much smaller than that of the deployed solar arrays, and therefore the radiation torque caused by the bus is an order of magnitude smaller than that caused by the arrays. For this reason and to conserve space the analytical details of derivation of the radiation torque on a bus will not be given here.

Torque On An Array Shadowed By the Spacecraft Bus

Fig. 5 portrays a spacecraft with a cylindrical bus and a solar array, the bus casting a shadow on the array. The lit semi-cylindrical surface is ABC. The shadow boundary on the array may utmost consist of three segments: an arc cast by the lit end-face of the cylinder and two straight lines, enclosing the arc, cast by the boundary rulings at A and C. The shadow in Fig. 5, though, has two segments only because the shadow of the ruling at A falls off the array. The shadow boundary is determined as follows

It may be clear that at any time only one array at the most will be shadowed. Knowing the angle β between the sun-ray unit vector $\underline{S}$ and nadir unit vector $\underline{c}_3$, we first determine which end-face is lit:

if $\beta < \pi/2$, the earth-pointing end-face is dark, and the opposite end-face is lit;

if $\beta > \pi/2$,the earth-pointing end-face is lit, and the opposite end-face is dark

and the lit semi-cylindrical surface is then identified. Next, let $\underline{r}$ be the vector from the reference origin O to any point P on the edge of the fully-lit face of the bus or along the two boundary rulings of the lit semi-cylinder. The vector from the hinge O_j of j^{th} array (j = 1,2) to the point P is then $-\underline{b}_j + \underline{r}$. The two components of this vector in the array plane $y_j z_j$, which is not necessarily normal to the sun, are

$$(-\underline{b}_j + \underline{r}) \cdot \underline{j}_j \qquad \text{and} \qquad (-\underline{b}_j + \underline{r}) \cdot \underline{k}_j \qquad (38)$$

where $\underline{j}_j$ and $\underline{k}_j$ are the unit vectors along y_j- and z_j-axis of the array, respectively. If these components fall on the array, that is,

$$a \le (-\underline{b}_j + \underline{r}) \cdot \underline{j}_j \qquad (39a)$$

$$-w/2 \le (-\underline{b}_j + \underline{r}) \cdot \underline{k}_j \le w/2 \qquad (j = 1,2) \qquad (39b)$$

where w is the width of the array along the z_j axis, then the array j is clearly shadowed. In that event, as the vector $\underline{r}$ moves along the edge of the lit end-face and the boundary rulings, the above two components will delineate the shadow boundary.

The radiation torque due to the array is still given by Eq. (17). The area A_j represents the lit area of the array, and the vector $\underline{\rho}_{pj}$ in the moment arm $\underline{c}_{pj}$, Eq. (16), is the vector from O_j to the instantaneous center of pressure of the shadowed array.

The instantaneous lit area and the vector $\underline{\rho}_{pj}$ are calculated numerically.

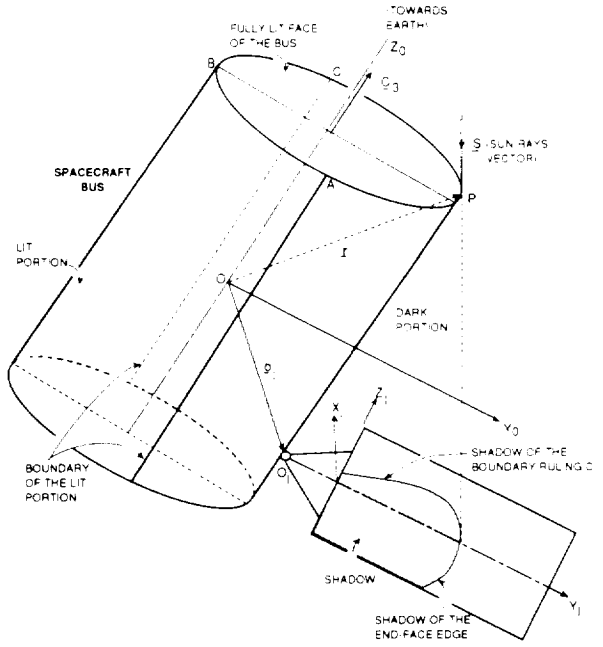

Fig. 5 Cylindrical Spacecraft Bus Casting Shadow on the Solar Array

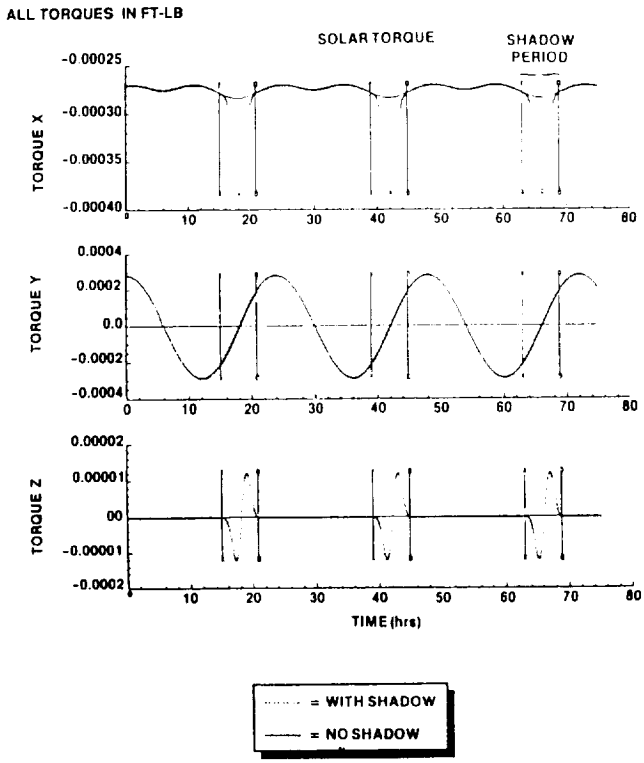

Fig. 6. Comparison of the total radiation torque on the spacecraft with and without considering the shadow; Orbital parameters: $\nu = 90°$, $\Omega_N = 180°$, $i = 20°$, corresponding solar arrays' inclinations: $\theta_{1z} = -\theta_{2z} = 43.5°$ (arrays parallel and both normal to the sun)

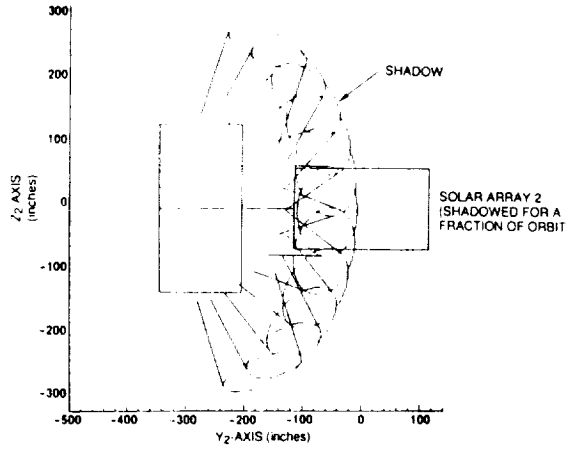

Fig. 7. Shadowing of –y array: Orbital Parameters and solar arrays' inclinations same as those in Fig. 6

Illustration

For parameters not recorded here because of space limitations, Fig. 6 furnishes total radiation torque (two arrays plus cylinder) with and without considering the shadow of the bus on the array, for $\underline{r}_c$=0 and both arrays normal to the sun rays. When the shadow is ignored, we observe that, in conformance with Eq. (36), the yaw torque is zero and the roll torque a constant over a few orbits. Slight oscillations in the roll torque are present because of the cylindrical bus. The variation of the pitch torque in Fig. 6 conforms with the y-component of the solar radiation torque in Eq. (36). Regarding the effect of shadow on the array, we observe that while the shadow does not alter y-torque, the trough of the x-torque plummets from –0.29E-3 ft.lb to –0.38E-3 ft.lb during the shadow period. A small (0.1E-4 ft.lb amplitude) cyclic z-torque also arises during the shadow period. For the parameters under consideration, it turns out that the –y-array is shadowed, +y-array is not. Traversal of the cylinder's shadow on the –y-array is shown in Fig. 7. The growth of the shadow area on the –y-array is shown in Fig. 8 for three parametric sets, including the set for Fig. 6. Fig. 8a shows that, for example, when θ_{2z} = –43.5°, the maximum shadow area equals 88 sq.ft [(shadow area) / (array area) = 88/202.85 = 0.43] and the array remains partially shadowed for nearly 6 hours (one-fourth of the orbital period). We nonetheless also observe that the shadow occupies 43% area of one array only briefly (several minutes), occupying progressively smaller area before and after the maximum shadow epoch. As the shadow traverses, the pressure center of the lit portion travels also; the loci of the instantaneous pressure center, from the moment the shadow enters the array till the moment it leaves, are shown in Fig. 8b for three sets of parameters. As expected, these loci are closed curves, and the bigger the angle $|\theta_{2z}|$, the wider the loci. The shadows occur around different orbit angles $\omega_0 t$ for different sets of orbital parameters v and Ω_N (even if the orbit inclination i is the same for these orbits). For plotting convenience, however, the maximum shadow epoch is shown to be the same (t = 18 hrs) in Fig. 8a for all three sets of parameters. In the preceding results, the center of mass vector $\underline{r}_c$ is zero. However, as the arrays orientations change relative to the spacecraft bus while

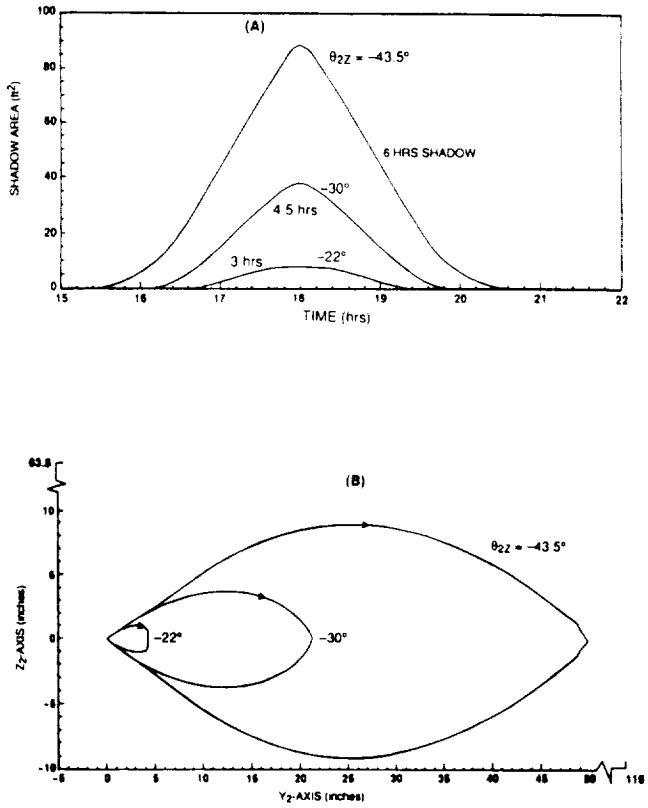

Fig. 8. (A) Shadow area on the –y-array versus time; (B) Locus of the pressure center of the –y-array as shadow travels on the array; orbital parameters for θ_{2z} = –43.5° the same as those in Fig.7; for θ_{2z} = –30°, the parameters are v = 30° and Ω_N = 140°; for θ_{2z} = –22°, v = 80°, Ω_N = 80°, and i = 20°

tracking the sun, $\underline{r}_c$ may vary depending on the arrays' arrangement. In the case at hand, this variation is found to be small, and it was *not* ignored in the computations.

The preceding results show that the spacecraft bus shadow on the array does not change radiation torque significantly. Also, based on the results not shown here due to space limitations and as stated before, the radiation torque on the bus is found to be an order of magnitude less than, and so negligible compared to, that on the arrays

4. Momentum Accumulation Due to Solar Radiation Torque

In the following analysis we will determine the momentum accumulation due to the arrays' torque only. It is instructive to compare the following development with that by McElvain[1].

Short Term Accumulation

Let $\underline{H}_b$ be the inertial angular momentum vector of the earth-pointing spacecraft under consideration. If H_x, H_y, H_z are the components of $\underline{H}_b$ in the body-fixed frame, then, in the presence of the radiation torque, (37d), they will be governed by the following three equations, expressed in the $\mathcal{F}^o$:

$$\dot{H}_x - \omega_0 H_z = g_c + g_a s\theta_{1y} \quad (40a)$$

$$\dot{H}_y = g_b c\theta_{1y} \quad (40b)$$

$$\dot{H}_z + \omega_0 H_x = g_a c\theta_{1y} \quad (40c)$$

As is well known, the roll (H_x) and yaw (H_z) momentums are gyrically coupled, whereas the pitch momentum (H_y) is independent of roll and yaw. Examining the definitions of g_a, g_b, g_c in Eqs. (37 a, b, c), we observe that they are functions of, among other things, the inclination angle θ_{1z} and the off-normal angle δ_{2z}. Because these angles depend on the earth's motion around the sun (the angle ν), they are held constant in flight over a few days, and therefore, within this period, the quantities g_a, g_b, g_c can be regarded as constant. Moreover, assuming that time t can be measured such that θ_{1y} (t=0) = 0, instead of θ_{10} according to Eq. (7), θ_{1y} (t) in Eq. (40) can be replaced with $\omega_0 t$. With these two assumptions, Eq. (40a) and (40c) can be integrated together, yielding ($i^2 = -1$)

$$H_x + iH_z = -i\,(g_c/\omega_0)\,(1-e^{-i\omega_0 t}) + i\,t\,g_a\,e^{-i\omega_0 t} \quad (41)$$

The integration of Eq. (40b), on the other hand, yields the pitch momentum H_y as

$$H_y\,(t) = (g_b/\omega_0)\,\sin\omega_0 t + H_{y0} \quad (42)$$

Because a constant torque g_c in the orbiting frame is a cyclic torque in the inertial frame, whereas a cyclic torque g_a in the orbit frame is a constant torque in the inertial frame, it is natural to find in Eq. (41) a cyclic variation in ($H_x + iH_z$) owing to g_c and a secular growth owing to g_a. At any arbitrary instant, the magnitude of the secular term in H_x+iH_z is tg_a, showing a linear growth in the spacecraft momentum in the roll-yaw plane. The pitch momentum H_y (t), Eq. (42), varies cyclically, with the amplitude equal to g_b/ω_0. The constant H_{y0} in Eq. (42) equals $H_y(0)$ and it embodies the spacecraft's y-momentum arising from its once-per-orbit equilibrium rotation.

Yearly Accumulation

It was just shown that the secular momentum in the roll-yaw plane at the end of one orbit ($\omega_0 t = 2\pi$) is ($H_x + iH_z$) = $i\,2\pi\,g_a/\omega_0$, where the coefficient g_a, Eq. (37b), is a function of the solar array's inclination angle θ_{1z} for an array normal to the sun, and of the inclination angles θ'_{2z} and off-normal angle δ_{2z} for an off-normal array. Fig. 3 shows that the angle θ_{1z} (or θ_{2z} which is equal to $-\theta_{1z}$) varies as a function of the angle ν (the earth's motion around the sun); therefore in order to calculate the yearly momentum accumulation, this variation must be considered. To separate the linearly varying angle ν(t), $0\le\nu\le2\pi$, from other constant orbital elements λ, Ω_N, and i in the definition of θ_{1z}, Eq. (8d) is rewritten thus:

$$\theta_{1z} = \sin^{-1}\,[\,(si\,s\Omega_N)\,c\nu + (-si\,c\Omega_N\,c\lambda + ci\,s\lambda)\,s\nu] \triangleq \sin^{-1}\,[A_0\,\sin\,(\nu_0 + \dot{\nu}t)] \quad (43)$$

with the amplitude A_0 and the phase angle ν_0 defined by:

$$A_0 = (A_s^2 + A_c^2)^{1/2} \le 1; \qquad \nu_0 = \tan^{-1}\,[A_s/A_c] \quad (44)$$

$$A_s = si\,s\Omega_N \qquad A_c = -si\,c\Omega_N\,c\lambda + ci\,s\lambda \quad (45)$$

Strictly speaking, because of orbit regression the ascending node angle Ω_N is not constant, but this variation is ignored here.

Spacecraft With +Y-Array Only; Array Normal to the Sun

When the +y-array is normal to the sun, the coefficient g_a given by Eq. (37b) simplifies to

$$g_a = pA_s\,\sigma_A\,(b + b_{1y}^{\oplus}\,c\theta_{1z}) \quad (46)$$

ignoring the second term in [•] in Eq. (37b) because it pertains to the −y-array. The magnitude of the secular momentum accumulated at any instant t then becomes

$$|H_x + iH_z| = pA_s\,\sigma_A\,(b + b_{1y}^{\oplus}\,c\theta_{1z})\,t \quad (47)$$

The yearly momentum is obtained by integrating (47) over the annual variation of the angle θ_{1z}. Let n_y be the current orbit under consideration:

$$n_y = t/\tau_0\,, \qquad \tau_0 \triangleq 2\pi/\omega_0 \quad (48)$$

where τ_0 is spacecraft orbit period, and let N_y be the total number of spacecraft orbits in one year. Then the yearly accumulation will be

$$H_{yr} = (pA_s\,\sigma_A\,\tau_0)\int_0^{N_y}(b + b_{1y}^{\oplus}\,c\theta_{1z})\,dn_y \quad (49)$$

Because $-\pi/2 < \theta_{1z} < \pi/2$, $c\theta_{1z}$ will always be positive. With the aid of Eq. (43) and recalling that b is constant (= $\ell/2$), and treating $b_{1y}^{\oplus}$, Eq. (22a), as constant, Eq. (49) transforms to

$$H_{yr} = (pA_s\,\sigma_A\,\tau_0)\,[bN_y + b_{1y}^{\oplus}\int_0^{N_y}\{1-A_0^2\,\sin^2(\nu_0 + \dot{\nu}\tau_0\,n_y)\}^{1/2}\,dn_y] \quad (50)$$

(The assumption $b_{1y}^{\oplus}$ a constant may not be always valid, because the quantity r_{cy} involved in the definition of $b_{1y}^{\oplus}$ may change due to θ_{1z}, but this change can be minimized by keeping the array's mass center on the axis of rotation.) Now, while n_y changes from 0 to N_y, the argument of $\sin^2$ in Eq. (50) varies from ν_0 to $\nu_0+2\pi$; therefore, the integral in (50) is an elliptic integral of the second kind. Measuring the time t such that the phase angle $\nu_0 = 0$ and capitalizing on the symmetry properties of the elliptic integral at hand, H_{yr} after integration is found to be

$$H_{yr} = (pA_s\,\sigma_A\,\tau_0)\,[bN_y + 4\,(b_{1y}^{\oplus}/\dot{\nu}\tau_0)\,E\,(\pi/2\,,\,A_0)] \quad (51)$$

where $E(\pi/2, A_0)$ is a complete elliptic integral given by the series:

$$\left[E(\pi/2, A_0) = (\pi/2) \left\{ 1 - \frac{1}{2^2} A_0^2 - \frac{1^2 \cdot 3}{2^2 \cdot 4^2} A_0^4 - \ldots - \left[\frac{(2n-1)!!}{2^n\, n!} \right]^2 \frac{A_0^{2n}}{2n-1} - \ldots \right\} \right] \tag{52}$$

Becasue the number of the spacecraft orbits in one year is

$$N_y = 2\pi/(\dot{\nu}\tau_0) \tag{53}$$

the yearly momentum accumulation H_{yr} simplifies to

$$H_{yr} = N_y\, \tau_0\, pA_s\, \sigma_A\, [b + b_{1y}{}^{\oplus} (1 - A_0{}^2/2^2 - \ldots)\,] \tag{54}$$

In the series (52) or (54), as many terms are retained as are necessary to evaluate the sum up to a desired accuracy.

Spacecraft With +Y and –Y Arrays:

a) Both Arrays Normal to the Sun

The coefficient g_a, Eq. (37b), now simplifies to

$$g_a = -2pA_s\, \sigma_A\, r_{cy}\, c\theta_{1z} \tag{55}$$

This is corroborated by the coefficient of $s\theta_{1y}$ in the first element of the vector equation (36). Comparing (55) with (46), the yearly momentum accumulation in the present case can be written down following Eq. (54):

$$H_{yr} = N_y\, \tau_0\, pA_s\, \sigma_A\, [\, -2r_{cy}\, (1 - A_0{}^2/2^2 - \ldots)] \tag{56}$$

b) +Y-Array Normal, –Y-Array Off-Normal to the Sun

In this case, the coefficient g_a is given by the full-length equation (37b). The definition of the coefficients b_c, b_s [Eq. (28)], and σ_{cx}, σ_{cy} [Eq. (32] reveal the presence of the products of the trigonometric functions of the angles θ'_{2z} and $\theta_{2z,a}$. The analysis therefore seems intractable, and developing a closed-form expression for H_{yr} infeasible; consequently, numerical integration of the equation $|H_x + iH_z| = t\, g_a$ over one year seems inevitable.

Yearly Propellant Consumption

Annual propellant consumption, W_p, should not be based on the momentum accumulation over one orbit and treating that constant for entire year, for the daily momentum varies significantly over one year (illustrated later in Fig. 10). Instead, knowing H_{yr} from Eq. (54), Eq. (56), or otherwise, and knowing the specific impulse I_{sp} of the propellant under consideration and moment arm ℓ_J of the thrusters from the vehicle mass center, W_p is obtained from

$$W_p = H_{yr} / (I_{sp}\, \ell_J) \tag{57}$$

Illustrations

Example 1. Spacecraft With Two Arrays: Momentum Accumulation Over Three Orbits

Fig. 9 illustrates momentum accumulation in the roll-yaw plane, Eq. (41), with the orbit angle $\omega_0 t$ as parameter. In particular, it applies to the spacecraft configuration shown in Fig. 4, with +y-array normal to the sun and –y-array off-normal at an angle δ_{2z}. Fig. 9 shows the linear, radial growth of $(H_x + iH_z)$—the term $itg_a\, e^{-i\omega_0 t}$ in Eq. (41)—superimposed upon a cyclic variation with an amplitude of g_c/ω_0.

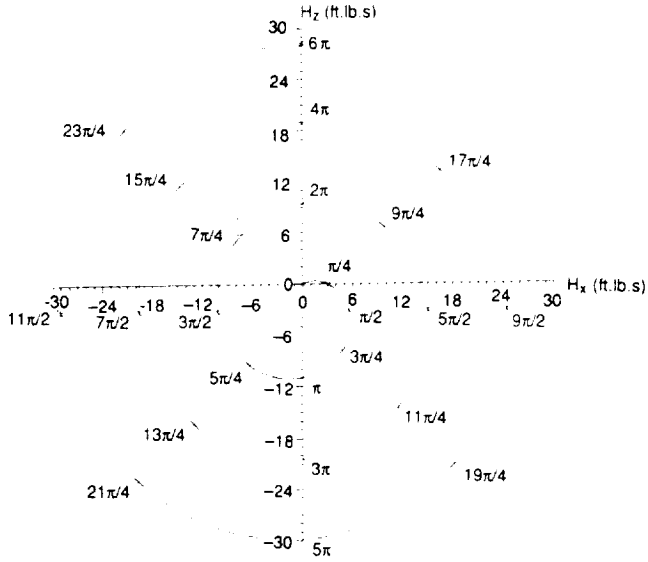

Fig. 9. Momentum accumulation in roll-yaw plane, due to the two arrays only: +Y array normal to the sun, $\theta_{1z} = -45°$; –Y array off-normal, $\theta_{2z}' = 25°$, $\delta_{2z} = 20°$, –Y array A-frame angle $\theta_{2z,a} = -37°$

Example 2. Momentum Accumulation As a Function of Earth's Position in the Ecliptic Plane

In order to obtain complete dependence of the daily momentum accumulation over a one year period, we next illustrate in Fig. 10 the roll-yaw momentum at $\omega_0 t = 2\pi$ and the pitch momentum amplitude g_b/ω_0 as a function of the angle ν: $0 \le \nu \le 2\pi$, with the off-normal angle δ_{2z} as a parameter. Figs. 10a and 10b show that, for off-normal angle $\delta_{2z} = 0$, the roll-yaw and pitch momentum amplitude varies periodically with ν, with half-year period; the corresponding ratio $H_y / |H_x + iH_z|$ remains constant for entire year. When the off-normal angle δ_{2z} of the –y-array is introduced, the half-yearly periodic variation of the roll-yaw momentum disappears and, instead, it begins to vary asymmetrically with ν. Also, the peaks and valleys of the roll-yaw momentum grow further apart as δ_{2z} increases. The half-year periodic variation of the pitch momentum amplitude alters little with the angle δ_{2z}. Fig. 10c illustrates the ratio $H_y / |H_x + iH_z|$; the variations in this ratio with ν become more pronounced as δ_{2z} increases. This ratio is of interest because it helps decide the cant angle of the reaction wheel configurations considered in the next section.

Example 3. Yearly Momentum Accumulation

When the off-normal angle δ_{2z} equals zero (that is, when both arrays are normal to the sun) the yearly momentum can be obtained analytically using Eq. (56), and when $\delta_{2z} \neq 0$, the yearly momentum is obtained by numerical integration of the

area under the curves $|H_x + iH_z|$ in Fig. 10a for the entire range $0 \le \nu \le 2\pi$. Fig. 11 depicts the yearly momentum against δ_{2z} for the range $0 \le \delta_{2z} \le 20°$ for different orbit inclination angles, keeping Ω_N at 170°. For $\delta_{2z} = 0$, the analytic prediction was compared and found identical with the numerical results. The number of terms that must be retained in the infinite series in Eq. (56) increases with the orbit inclination i, and yearly momentum diminishes a little. The yearly momentum, however, increases significantly with the off-normal angle δ_{2z}, as seen in Fig. 11.

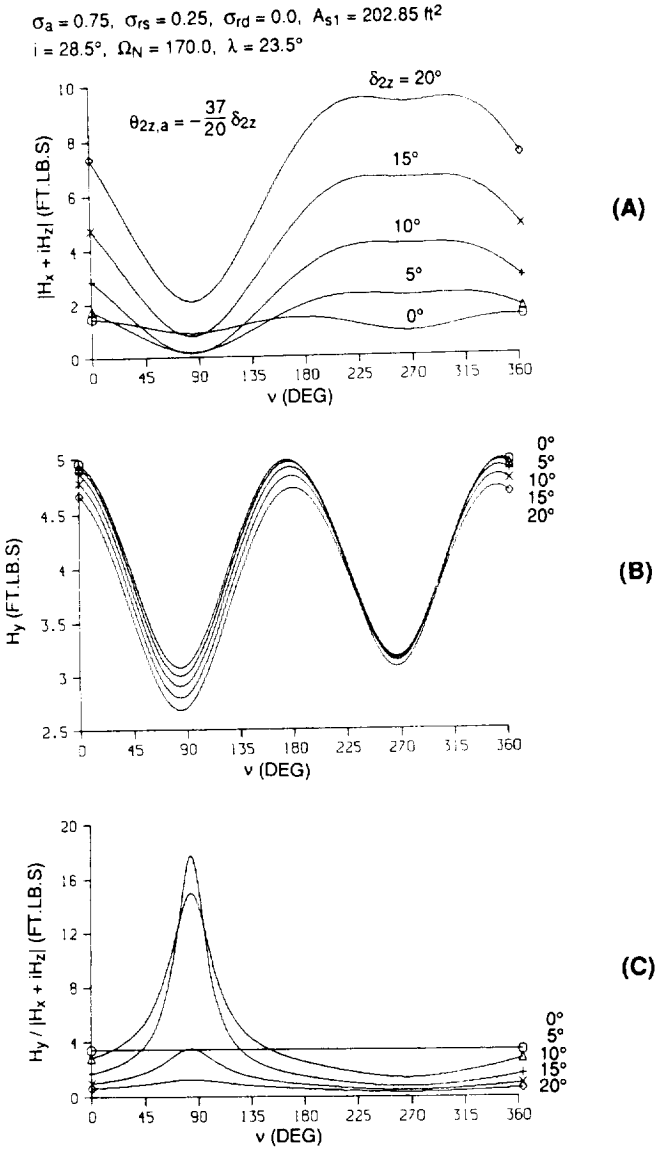

Fig. 10. Variation of roll-yaw and pitch momentum with the earth's position (the angle ν) in the ecliptic plane; y-array normal to the sun, –y-array off-normal at an angle δ_{2z} and its A-frame at an angle $\theta_{2z,a}$; $\lambda = 23.44°$, orbit ascending node angle $\Omega_N = 170°$, and inclination angle $i = 28.5°$

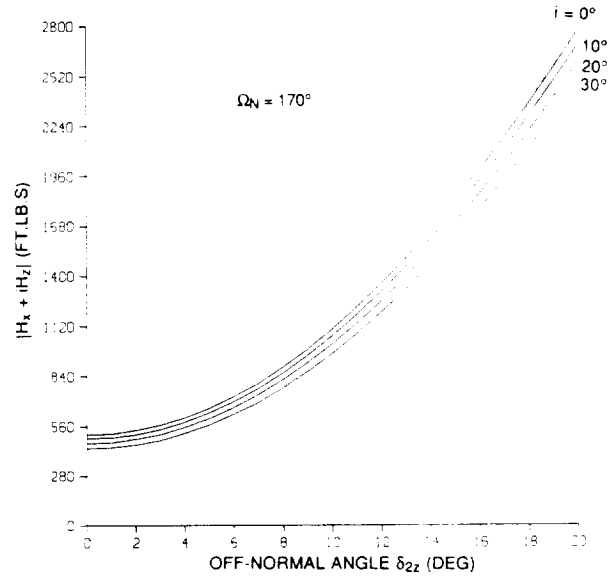

Fig. 11. Annual roll-yaw momentum versus off-normal angle of –y-array; +y-array always normal to the sun; $\Omega_N = 170°$

5. Reaction Wheel Sizing and Configuration Optimization

In Section 4, we observed that the momentum along the roll and yaw axes are coupled. Depending on the initial conditions, the secular momentum build-up tg_a can exceed the capacity of the wheels either about the roll-axis, yaw-axis, or any other direction in the roll-yaw plane. Therefore, for the design purposes, the desired momentum capacity in the roll-yaw plane is the same in all directions. In contrast, the pitch momentum caused by the radiation torque is cyclic, with the amplitude equal to (g_b/ω_0). Hence, the pitch and roll-yaw momentum requirements leads to the well-known right circular cylinder momentum requirement for designing a wheel configuration, with cylinder axis along the pitch axis. On the other hand, the reaction wheels are also required to produce certain peak control torque about each of the three spacecraft axes. The torque requirements therefore form a rectangular parallelepiped. Both the momentum and the torque requirements can be met, in principle, using three wheels (not necessarily an orthogonal set); but for the sake of redundancy, four or more are often employed. In the following subsections, four-, six-, and three-wheel configurations are analyzed, two arrangements of the wheels and one-wheel failure are considered for each configuration.

To visualize the wheel configuration most easily, first place the spin axes of all the wheels in the roll-yaw plane, perhaps radially symmetrically along the roll and yaw axes or otherwise, and then cant all spin axes, equally or unequally depending on the design, towards the pitch axis or its opposite. When the wheels are not along the spacecraft axes, a transformation matrix $\underline{C}_{bw}$ is required to transform the wheel momentum vector $\underline{H}_{ww}$ along the wheel axes to the total wheel momentum $\underline{H}_{bw}$ along the spacecraft axes:

$$\underline{H}_{bw} = \underline{C}_{bw}\,\underline{H}_{ww} \tag{58}$$

When the number of wheels, n_w, is more than 3, the matrix $\underline{C}_{bw}$ is rectangular, $3xn_w$, and its pseudo-inverse $\underline{C}_{bw}^{\dagger}$

$$\underline{C}_{bw}^{\dagger} = \underline{C}_{bw}^{T} (\underline{C}_{bw} \underline{C}_{bw}^{T})^{-1} \tag{59}$$

is required for the inverse transformation of (58):

$$\underline{H}_{ww} = \underline{C}_{bw}^{\dagger} \underline{H}_{bw} \tag{60}$$

The above two transformation matrices are useful also for transforming the desired control torque $\underline{T}_c$ (3x1) about the spacecraft axes to the desired rate of change of the wheel angular momentum vector $\dot{\underline{H}}_{ww}$ (n_w x 1):

$$\dot{\underline{H}}_{ww} = - \underline{C}_{bw}^{\dagger} \underline{T}_c \tag{61}$$

To determine the optimum cant angle(s) with the roll-yaw plane, it is logical to impose the requirement that, for a desired momentum vector capacity $\underline{H}_{bw}$ in spacecraft axes, the norm of the wheel momentum vector $\underline{H}_{ww}$ be the least so as to minimize the cost and weight of the wheels. One suitable norm of the vector $\underline{H}_{ww}$ is its Euclidean norm $\| \underline{H}_{ww} \|$ defined by

$$\| \underline{H}_{ww} \| = \left[\sum_{i=1}^{n_w} H_{wi}^2 \right]^{1/2} \tag{62}$$

where H_{wi} ($i = 1, ..., n_w$) are the elements of the vector $\underline{H}_{ww}$. The minimization of $\| \underline{H}_{ww} \|$ also results in minimum power consumption by the wheels for controlling the spacecraft, as shown below.

Let $\omega_{wi}(0)$ be the initial speed of the wheel i, and $\omega_{wi}(t)$ the instantaneous speed while the wheel is acted upon by an electric motor, changing the wheel's momentum H_{wi} at the rate $\dot{H}_{wi}(t)$. Then

$$\omega_{wi}(t) = \omega_{wi}(0) + I_w^{-1} \int \dot{H}_{wi}(t)\, dt \tag{63}$$

where I_w equals wheel's moment of inertia about the spin-axis. For a constant $\dot{H}_{wi}$, the instantaneous power P_{wi} consumed by the wheel i is given by,

$$P_{wi} = | \dot{H}_{wi} | \, | \omega_{wi}(0) + I_w^{-1} \dot{H}_{wi} \, t | \tag{64}$$

where absolute values are taken to ensure that the power P_{wi} is positive for both signs of $\dot{H}_{wi}(t)$ and $\omega_{wi}(t)$. To determine the worst power consumption by the wheel assembly, we assume that $\omega_{wi}(0)$ has the same sign as that of $\dot{H}_{wi}$. Furthermore, assuming that $\omega_{wi}(0)$ is the same for all wheels, the total power P_w consumed by the n_w wheels will be

$$P_w = | \omega_w(0) | \sum_{i=1}^{nw} | \dot{H}_{wi} | + t\, I_w^{-1} \| \dot{\underline{H}}_{ww} \|^2 \tag{65}$$

Thus, we see that, ignoring the linear term, minimization of power consumption leads to the minimization of the norm $\| \dot{\underline{H}}_{ww} \|$.

The vectors $\underline{H}_{ww}$ and $\dot{\underline{H}}_{ww}$ are related, respectively, to the required momentum capacity $\underline{H}_{bw}$ and the control torque capacity $\underline{T}_c$ through the same pseudo-inverse matrix $\underline{C}_{bw}^{\dagger}$. Therefore, the minimization of both $\underline{H}_{ww}$ and $\dot{\underline{H}}_{ww}$ yields the same optimum cant angle if the components of $\underline{H}_{bw}$ and $\underline{T}_c$ are proportional. This condition, however, is not always obeyed; for instance, in the presence of radiation torque, the desired roll and yaw momentum requirements are the same, but the desired roll and yaw torque requirements may be different because the roll and yaw errors might be controlled with controllers of different bandwidths, and the corresponding moments of inertia might be quite different. As a different example, the roll and yaw torques limits could be the same to facilitate momentum dumping with thrusters. The need for deliberation is thus evident.

Four-Wheel Pyramid Configurations

One possible arrangement of four wheels is shown in Fig. 12. The angle between two adjacent wheels is 90°, and they all are equally canted toward the –y axis by an angle η measured from the roll-yaw plane. When the cant angle η and the angle γ in the roll-yaw plane are both zero, the momentum h_1 of the wheel 1 is along the z-axis, h_2 along the x-axis, h_3 opposite to h_1, and h_4 opposite to h_2. The angle γ is introduced so that the wheel torque can contribute, if desired, to all three axes and not just to roll and pitch or yaw and pitch. The corresponding rectangular matrix $\underline{C}_{bw}$ is

$$\underline{C}_{bw} = \begin{bmatrix} c\eta s\gamma & c\eta c\gamma & -c\eta s\gamma & -c\eta c\gamma \\ -s\eta & -s\eta & -s\eta & -s\eta \\ c\eta c\gamma & -c\eta s\gamma & -c\eta c\gamma & c\eta s\gamma \end{bmatrix} \tag{66}$$

whose pseudo-inverse, Eq. (59), is found to be

$$\underline{C}_{bw}^{\dagger} = \begin{bmatrix} s\gamma/2c\eta & -1/4s\eta & c\gamma/2c\eta \\ c\gamma/2c\eta & -1/4s\eta & -s\gamma/2c\eta \\ -s\gamma/2c\eta & -1/4s\eta & -c\gamma/2c\eta \\ -c\gamma/2c\eta & -1/4s\eta & s\gamma/2c\eta \end{bmatrix} \tag{67}$$

Let H_x, H_y, H_z be the desired momentum capacity of the reaction wheels about the roll-, pitch-, and yaw-axis of the spacecraft. These three components disperse along the four wheel axes as follows, using Eqs. (60) and (67):

$$\underline{H}_{ww} = \begin{bmatrix} (H_x s\gamma + H_z c\gamma)/2c\eta & - H_y/4s\eta \\ (H_x c\gamma - H_z s\gamma)/2c\eta & - H_y/4s\eta \\ (-H_x s\gamma - H_z c\gamma)/2c\eta & - H_y/4s\eta \\ (-H_x c\gamma + H_z s\gamma)/2c\eta & - H_y/4s\eta \end{bmatrix} \tag{68}$$

Let, T_x, T_y, T_z be the desired maximum control torques about the x-, y-, and z-axis of the spacecraft. The maximum rate of change of the wheel angular momentum about wheel axes is then, according to Eqs. (61) and (67)

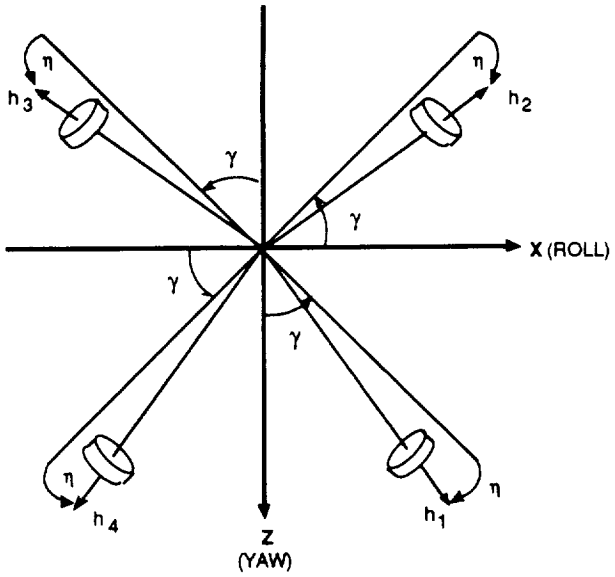

Fig. 12. Four-Wheel Configuration

$$\dot{\underline{H}}_{ww} = \begin{bmatrix} (-T_x s\gamma - T_z c\gamma)/2c\eta & + T_y/4s\eta \\ (-T_x c\gamma + T_z s\gamma)/2c\eta & + T_y/4s\eta \\ (\ T_x s\gamma + T_z c\gamma)/2c\eta & + T_y/4s\eta \\ (\ T_x c\gamma - T_z s\gamma)/2c\eta & + T_y/4s\eta \end{bmatrix} \qquad (69)$$

If H_x, H_y, H_z are the desired momentum capacity of the reaction wheels about the roll, pitch, and yaw axis of the spacecraft, the 4x1 vector $\underline{H}_{ww}$ is calculated analogously. Based on the definition (62), the norms $\| \underline{H}_{ww} \|$ and $\| \dot{\underline{H}}_{ww} \|$ are then found to be:

$$\| \underline{H}_{ww} \|^2 = (H_x^2 + H_z^2) / (2c^2\eta) + H_y^2 / (4s^2\eta) \qquad (70)$$

$$\| \dot{\underline{H}}_{ww} \|^2 = (T_x^2 + T_z^2) / (2c^2\eta) + T_y^2 / (4s^2\eta) \qquad (71)$$

which are independent of the angle γ because the angle between two adjacent wheels is 90°. Comparing the two norms, it is clear that if (H_x, H_y, H_z) and (T_x, T_y, T_z) are proportional,the minimization of one is the minimization of the other. The optimum cant angle η^* is found to be

$$\tan^4 \eta^* = H_y^2/2(H_x^2 + H_z^2) = T_y^2/2(T_x^2 + T_z^2) \qquad (72)$$

which may be rewritten in a more revealing form:

$$T_x^2/\ T_y^2 + T_z^2/\ T_y^2 = 1/(2\tan^4 \eta^*) \qquad (73)$$

which is the equation of a circle in the plane ($T_x/\ T_y$, $T_z/\ T_y$) and the radius of the circle equals $1/(\sqrt{2}\ \tan^2 \eta^*)$. Eq. (73) states that as the torque requirements about x- and z-axis diminish, the radius of the circle shrinks and the optimum cant angle η^* increases. This is exemplified in Fig.13 where Eq. (73) is plotted for $\eta^* = 25°, 30°, ..., 60°$.

The norm $\| \dot{\underline{H}}_{ww} \|$ can be made dimension-free by dividing Eq. (71) with T_y^2. This dimension-free right side of Eq. (71) is plotted in Fig. 14 as a function of η for a given $(T_x^2 + T_z^2)/T_y^2$. The minimum value of the norm occurs at the optimum cant angle η^*, and that minimum norm is found to be

$$\| \dot{\underline{H}}_{ww} \|^2_{min} / T_y^2 = [\ \sqrt{2}\ (\sigma_{xy}^2 + \sigma_{zy}^2)^{1/2} + 1\ ]^2/4 \qquad (74)$$

where the torque ratios σ_{xy} and σ_{zy} are defined as

$$\sigma_{xy} = T_x / T_y \qquad \sigma_{zy} = T_z / T_y \qquad (75)$$

Table 2 furnishes optimum cant angle η^* for several desired torque ratios; it also demonstrates that, for example, $\eta^* = 35.26$ as long as $\sigma_{xy}^2 + \sigma_{zy}^2 = 2$, regardless of the individual values of σ_{xy} and σ_{zy}.

To determine the torque (or momentum) capacity of the wheels to produce the desired maximum torques (or momentums) along the spacecraft axes, we again consider $\dot{\underline{H}}_{ww}$, Eq. (69). Because T_x, T_y, T_z are only *three* independent torque requirements, the *four* elements of $\dot{\underline{H}}_{ww}$ are not all independent. Indeed, they are constrained by a relationship that is divulged from

$$\dot{\underline{H}}_{ww} = \underline{C}_{bw}^{\dagger}\, \underline{C}_{bw}\, \dot{\underline{H}}_{ww}, \qquad (76)$$

$$(T_x / T_y)^2 + (T_z / T_y)^2 = 1/(2\mathrm{TAN}^4\eta)$$

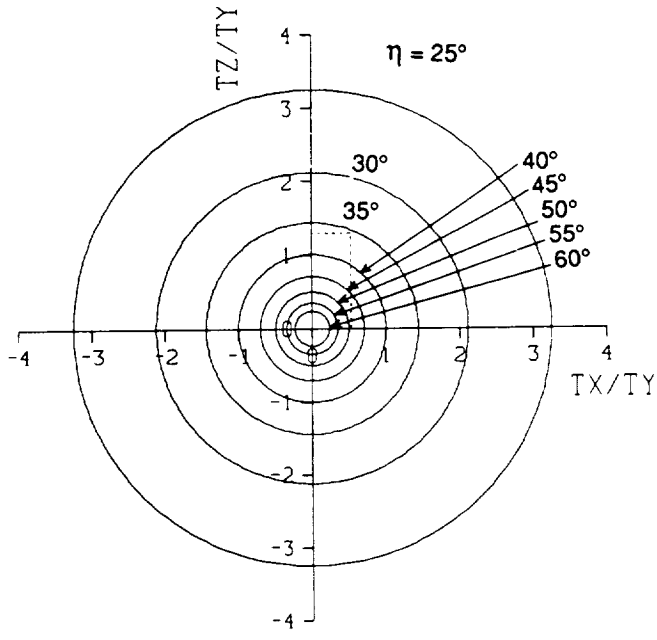

Fig. 13. Dependence of minimum-power cant angle on desired torque ratios

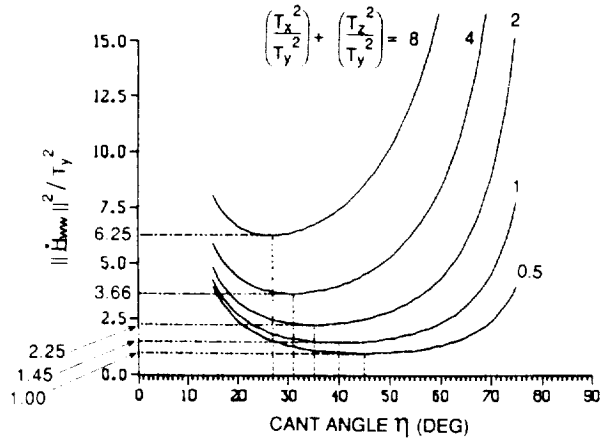

Fig. 14. $\|\dot{H}_{ww}\|^2 / T_y^2$ versus cant angle η for a four-wheel configuration

Table 2. Examples of dependence of optimum cant angle on the desired torque ratios(σ_{xy} and σ_{zy})

$(T_x/T_y)^2 + (T_z/T_y)^2$	Optimum Cant Angle	Example Ratios	
		T_x/T_y	T_z/T_y
0.5	45°	0.5	0.5
1	40.06°	$1/\sqrt{2}$	$1/\sqrt{2}$
2	35.26°	1 0 $\sqrt{2}$	1 $\sqrt{2}$ 0
4	30.73°	$\sqrt{2}$	$\sqrt{2}$
8	26.56°	2	2

Recalling (66) and (67), Eq. (76) yields four identical equations stating

$$\dot{H}_{w1} + \dot{H}_{w3} = \dot{H}_{w2} + \dot{H}_{w4} \tag{77}$$

The wheel momentums observe a similar relationship.

Because of (77) and because of the nature of decomposition of the three desired torques T_x, T_y, T_z along the four wheel axes, Eq. (69), it may be intuitively clear that the magnitude of each element in (69) will not simultaneously reach $\dot{H}_{w,max}$—the maximum achievable rate of change of wheel's angular momentum. Therefore, recalling the definition (62)

$$\| \underline{\dot{H}}_{ww} \|^2 < 4\dot{H}_{w,mx}^2 \tag{78}$$

When the cant angle is optimum, the norm $\| \underline{\dot{H}}_{ww} \|$ is related to the specified torques T_x, T_y, T_z according to Eq. (74). Therefore, in view of (78)

$$[\sqrt{2}\,(T_x^2 + T_z^2)^{1/2} + T_y\,]/4 < \dot{H}_{w,mx} \tag{79}$$

By way of illustration, if the torque requirements about the three axes are all equal ($T_x = T_y = T_z$), the inequality (79) yields

$$\dot{H}_{w,mx} > 3T_x/4 \tag{80}$$

Considering that there are four wheels, each of capacity $\dot{H}_{w,mx}$, for controlling three axes of the spacecraft each requiring the torque T_x, the inequality (80) is perhaps a natural result, but it does not reveal just how much $\dot{H}_{w,mx}$ must at last be, to size the wheel. For that, the Euclidean norm is not helpful and we must focus on Eq. (69) itself, as illustrated in the following two illustrations.

Wheels Contributing to Roll and Pitch or Yaw and Pitch Only

In Fig. 12, when γ = 0 or 90°, each wheel contributes to either roll and pitch or yaw and pitch axes only. Regardless of γ, the optimum cant angle for equal torque and momentum requirements satisfies, according to Eq. (72):

$$\eta^* = 35.26°, \quad \tan\eta^* = 1/\sqrt{2}, \quad \sin\eta^* = 1/\sqrt{3}, \quad \cos\eta^* = \sqrt{2/3} \tag{81}$$

Substituting $T_x = T_y = T_z$ and $s\eta^*$ and $c\eta^*$ from (81) in (69), we obtain, for γ = 90°

$$\underline{\dot{H}}_{ww} = T_x\,[\,-0.179 \quad 1.045 \quad 1.045 \quad -0.179\,]^T \tag{82a}$$

which yields the desired maximum wheel torque capacity when not one wheel has failed

$$\dot{H}_{w,mx} \geq 1.045\,T_x \tag{82b}$$

It is illuminating to compare the inequality (80) with (82b).

Regarding the required momentum capacity of the wheels, we first obtain $\underline{H}_{ww}$, from Eq. (60), for γ = 90°. Next, recall that from Eq. (41), the secular roll or yaw momentum at the end of one orbit is $g_a\tau_0$ (τ_0 = orbital period) and, from Eq. (42), the pitch momentum amplitude is g_b/ω_0. The least momentum capacity of a wheel for momentum dumping per orbit and for optimum cant angle (81) is then

$$H_{w,mx} \geq \sqrt{3}\,|g_a|\tau_0 / 2\sqrt{2} + \sqrt{3}\,|g_b| / 4\omega_0 \tag{83}$$

Finally, in order to calculate the power consumption P_w versus time t, Eq. (65), we require the quantities $\sum_{i=1}^{nw} |\dot{H}_{wi}|$ and $\| \underline{\dot{H}}_{ww} \|^2$. From Eq. (82a),

$$\sum_{i=1}^{nw} |\dot{H}_{wi}| = 2.449\,T_x \tag{84a}$$

which determines the intercept of the P_w versus t curve at t = 0. The slope of this curve is proportional to the norm $\| \underline{\dot{H}}_{ww} \|^2$

which, for equal torque requirement, is obtained from Eq. (74) by inserting $\sigma_{xy} = 1 = \sigma_{yz}$:

$$\| \dot{\underline{H}}_{ww} \|^2 = 2.25\ T_x^2 \qquad (84b)$$

The indexes (84a) and (84b) should be kept as small as consistent with performance specifications.

Wheels Contributing to All Three Axes

In Fig. 12, when $\gamma = 45°$, each of the four wheels contributes equally to the roll and yaw axes, as evident from Eq. (69). Reference 6 has examined this configuration to some depth. For $\gamma = 45°$, for equal torque requirements ($T_x = T_y = T_z$) and optimum cant angle (81), Eq. (69) yields

$$\dot{\underline{H}}_{ww} = T_x [\ -\sqrt{3}/4 \qquad \sqrt{3}/4 \qquad 3\sqrt{3}/4 \qquad \sqrt{3}/4\ ]^T \qquad (85a)$$

The element with maximum absolute value yields the desired torque capacity of the wheel:

$$\dot{H}_{w,mx} \geq 3\sqrt{3}\ T_{mx}/4 = 1.3\ T_x \qquad (85b)$$

Comparing (85b) with (82), we conclude that, to produce a torque of magnitude T_x about each of the three axes, the reaction wheels corresponding to $\gamma = 45°$ configuration must have 24.4% higher torque capacity than the wheels corresponding to $\gamma = 0°$ configuration. This is not surprising because for $\gamma = 45°$, the wheel's torque capacity is dispersed along all three axes, whereas in the case $\gamma = 0°$, it is distributed along roll and pitch or yaw and pitch only.

Following the derivation of the wheel momentum capacity, Eq. (83), the desired capacity for the configuration at hand is

$$H_{w,mx} \geq \sqrt{3}\ (\ |g_a|\ \tau_0 + |g_b|\ /\ \omega_0\ )/4 \qquad (86)$$

where the optimum cant angle (81) has been used. Comparing (86) with (83), we find that $H_{w,mx}$ now ($\gamma = 45°$) is smaller than before ($\gamma = 0°$), in contrast with the torque capacity conclusion drawn above. The reason of course is that the secular momentum $\tau_0 g_a$ is either about the roll-axis or yaw-axis, not both, whereas the torque capacity T_x is desired about both roll and yaw axes.

The two indexes of the power consumption are calculated with the aid of (85a) and (74):

$$\sum_{i=1}^{4} |\ \dot{H}_{wi}\ | = 2.598\ T_x \qquad (87a)$$

$$\| \dot{\underline{H}}_{ww} \|^2 = 2.25\ T_x^2 \qquad (87b)$$

Comparing (87a) with (84a) and (87b) with (84b), we conclude that, for producing equal torque about the three spacecraft axes, and for the same initial wheel speed, the $\gamma = 45°$ wheel-configuration begins with a slightly higher power consumption and increases at the same rate as the $\gamma = 90°$ or $0°$ configuration.

One-Wheel Failure

For the four-wheel configuration shown in Fig. 12, we are usually interested in either $\gamma = 45°$ or $90°$ ($\gamma = 0°$ or $90°$ are effectively the same). And for these values, because all wheels are arranged symmetrically, failure of any wheel has the same consequences as the failure of any other. Therefore, to facilitate analysis, we arbitrarily assume the failure of wheel-3, and in that case the 3x4 transformation matrix $\underline{C}_{bw}$, Eq. (66), condenses to a 3x3 matrix $\underline{C}_{bw,3}$, formed by deleting the third column of $\underline{C}_{bw}$. The inverse $\underline{C}_{bw,3}^{-1}$ of $\underline{C}_{bw,3}$ is found and then used to determine the torque vector $\dot{\underline{H}}_{ww}$, following (61):

$$\dot{\underline{H}}_{ww} = \begin{bmatrix} -T_x s\gamma/c\eta & & -T_z c\gamma/c\eta \\ T_x(s\gamma - c\gamma)/2c\eta + T_y/2s\eta + T_z(s\gamma + c\gamma)/2c\eta & & \\ 0\ (\text{wheel-3 failed}) & & \\ T_x(s\gamma + c\gamma)/2c\eta + T_y/2s\eta - T_z(s\gamma - c\gamma)/2c\eta & & \end{bmatrix} \qquad (88)$$

The wheel momentum vector $\underline{H}_{ww}$ is determined likewise. For one-wheel failure case, the cant angle is not re-optimized because the cant angle of the wheels, once installed, is not changeable in the flight.

Maximum Torque and Momentum Capacity When $\gamma = 90°$

For $\gamma = 90°$, and for the optimum cant angle (81), Eq. (88) yields

$$\dot{\underline{H}}_{ww} = T_x [-1.225 \quad 2.091 \quad 0 \quad 0.866]^T \qquad (89a)$$

which in turn yields the required torque capacity of the wheel as

$$\dot{\underline{H}}_{w,mx} \geq 2.091\ T_x \qquad (89b)$$

This is twice the required torque capacity in the no-failure case, Eq. (82b).

Following the derivation of the momentum capacity Eq. (83) for the no-failure case, the momentum capacity for one-wheel failure case is:

$$\underline{H}_{ww} = \begin{bmatrix} \sqrt{3}\ |g_a|\ \tau_0/\sqrt{2} \\ \sqrt{3}\ |g_a|\ \tau_0/2\sqrt{2} + \sqrt{3}\ |g_b|\ /2\omega_0 \\ 0\ (\text{wheel-3 failed}) \\ \sqrt{3}\ |g_a|\ \tau_0/2\sqrt{2} + \sqrt{3}\ |g_b|\ /2\omega_0 \end{bmatrix} \qquad (90)$$

Depending upon the relative magnitudes of g_a and g_b, either wheel-1 or wheel-2 will yield the required momentum capacity (wheel-4 will yield the same capacity as the wheel-2).

Regarding the two indexes of power consumption, Eq. (89a) furnishes

$$\sum_{i=1}^{4} | \dot{H}_{wi} | = 4.182\, T_x \qquad (91a)$$

$$\| \underline{\dot{H}}_{ww} \|^2 = 6.62\, T_x^2 \qquad (91b)$$

which may be compared with the no-failure results, Eqs. (87).

Maximum Torque and Momentum Capacity When $\gamma = 45°$

For equal torque requirements about the roll, pitch, and yaw axes ($T_x = T_y = T_z$), and for the optimum cant angle $\eta^* = 35.26$, the desired torque capacity of each wheel is

$$\dot{H}_{w,mx} \geq 1.732\, T_x \qquad (92)$$

juxtaposed to the no-failure size (85b). By comparing the size (92) with the size (89b), the advantage of $\gamma = 45°$ configuration over $\gamma = 0°$ or $90°$ configuration emerges: when one wheel fails, the $\gamma = 45°$ configuration can control the spacecraft with the wheels of smaller torque capacity than the $\gamma = 0°$ or $90°$ configuration can.The two indexes of power consumption are:

$$\sum_{i=1}^{4} | \dot{H}_{wi} | = 3\sqrt{3}\, T_x = 5.196\, T_x$$

$$\| \underline{\dot{H}}_{ww} \|^2 = 9\, T_x^2 \qquad (93b)$$

Comparing (93) with (91), a disadvantage of the $\gamma = 45°$ configuration is also unveiled: its power consumption is significantly greater than that of the $\gamma = 90°$ configuration. Finally, the desired momentum capacity is

$$H_{w,mx} = \sqrt{3}\, (|g_a|\, \tau_0 + |g_b| / \omega_0) /2 \qquad (94)$$

Compared with its no-failure counterpart, Eq. (86), the desired momentum capacity is now twice.

Reference 6 may be reviewed for a different aspect regarding the selection of cant angle for the configuration at hand.

Six-Wheel Pyramid Configurations

Two-Cant-Angle Configuration

One such configuration is shown in Fig. 15 where the wheels are arranged symmetrically ($\gamma = 60°$), wheels 2 and 5 controlling roll and pitch axes, and wheels 1, 3, 4, and 6 controlling all three axes. Because of this fundamental difference between the two subsets of wheels, the cant angle η_2 of the former subset is allowed to be, in general, different from the cant angle η_1 of the latter subset. This freedom permits a greater economy in power consumption, if desired, and allows the reaction wheels to be of smaller torque and momentum capacity than the one-cant-angle configuration does.

To determine the optimum cant angles η_1^* and η_2^*, define

$$c_i = \cos \eta_i \qquad s_i = \sin \eta_i \qquad (i = 1,2) \qquad (95)$$

The transformation matrix $\underline{C}_{bw}$ (3x6) is

$$\underline{C}_{bw} = \begin{bmatrix} c_1/2 & c_2 & c_1/2 & -c_1/2 & -c_2 & -c_1/2 \\ -s_1 & -s_2 & -s_1 & -s_1 & -s_2 & -s_1 \\ \sqrt{3}c_1/2 & 0 & -\sqrt{3}c_1/2 & -\sqrt{3}c_1/2 & 0 & \sqrt{3}c_1/2 \end{bmatrix} \qquad (96)$$

where, from the second and fifth column, it is apparent that the wheels 2 and 5 do not control the yaw axis, while the remaining four wheels control all axes. The pseudo-inverse matrix $\underline{C}_{bw}^{\dagger}$ is determined using the definition (59):

$$\underline{C}_{bw}^{\dagger} = \begin{bmatrix} \begin{Bmatrix} c_1/2 \\ c_2 \\ c_1/2 \\ -c_1/2 \\ -c_2 \\ -c_1/2 \end{Bmatrix} /(c_1^2 + 2c_2^2) & \begin{Bmatrix} -s_1 \\ -s_2 \\ -s_1 \\ -s_1 \\ -s_2 \\ -s_1 \end{Bmatrix} /(4s_1^2 + 2s_2^2) & \begin{Bmatrix} 1 \\ 0 \\ -1 \\ -1 \\ 0 \\ 1 \end{Bmatrix} /2\sqrt{3}c_1 \end{bmatrix} \qquad (97)$$

and the Euclidean norm of the vector $\underline{\dot{H}}_{ww}$ is

$$\| \underline{\dot{H}}_{ww} \|^2 = T_x^2/(c_1^2 + 2c_2^2) + T_y^2/2(2s_1^2 + s_2^2) + T_z^2/3c_1^2 \qquad (98)$$

which is minimized by the optimum angles η_1^* and η_2^* defined by

$$s^2\eta_1^* = (T_x + T_y - T_z) / (T_x + T_y + T_z),$$
$$c^2\eta_1^* = 2T_z / (T_x + T_y + T_z) \qquad (99a)$$

$$s^2\eta_2^* = \{2(T_z - T_x) + T_y\} / (T_x + T_y + T_z),$$
$$c^2\eta_2^* = (3T_x - T_z) / (T_x + T_y + T_z) \qquad (99b)$$

Fig. 16 portrays the optimum angles η_1^* and η_2^* for specified torque ratios σ_{xz} and σ_{yz}. Substituting the optimum trigonometric functions in Eq.(98), the minimum value of the norm $\| \underline{\dot{H}}_{ww} \|^2$ is found to be

$$\| \underline{\dot{H}}_{ww} \|^2 = (T_x + T_y + T_z)^2 /6 \qquad (100)$$

The three torque components T_x, T_y, T_z are independent, and once specified, they are produced by the six $\dot{H}_{wi}$ (i=1, ..., 6), given by Eq. (61). Clearly, these six quantities are constrained by three relations which are obtained from the expanded version of Eq. (76). Due to these constraints,

$$\| \underline{\dot{H}}_{ww} \|^2 < 6\, \dot{H}_{w,mx}^2 \qquad (101)$$

analogous to the inequality (78) for the 4-wheel configurations. Combining (101) with (100), we obtain

$$(T_x + T_y + T_z) / 6 < \dot{H}_{w,mx} \qquad (102)$$

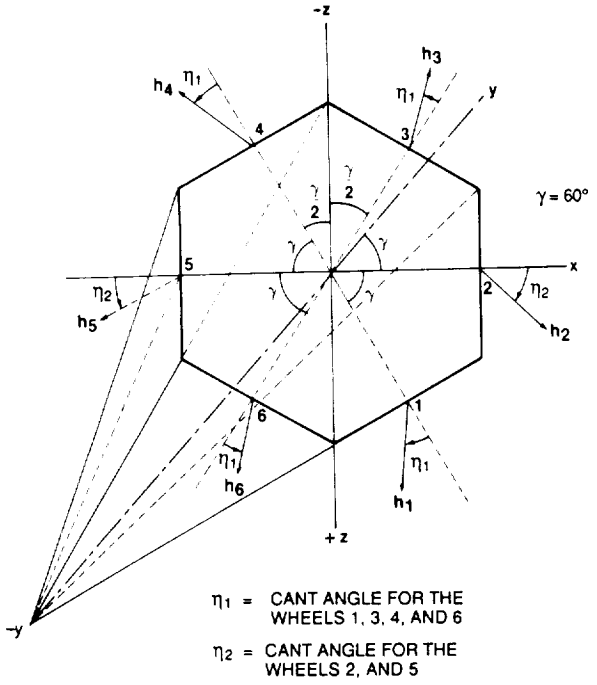

Fig. 15. Six-wheel hexagonal configuration

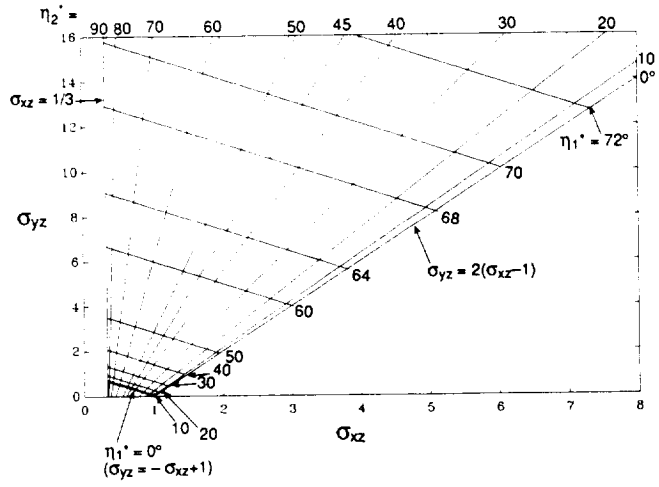

Fig. 16. Dependence of optimum cant angles η_1^* and η_2^* on the torque ratios σ_{xz} and σ_{yz}

which states that the sum of the maximum torques that can be produced about the three spacecraft axes must be less than the total torque capacity of the wheels—the cant angles being the underlying reason. For equal torque requirements ($T_x = T_y = T_z$), the inequality (102) reduces to

$$\dot{H}_{w,mx} > T_x/2 \qquad (103)$$

which may be compared with (80). It is intuitively clear that, instead of arranging six wheels as shown in Fig. 15, if they were arranged two wheels per axis, then for equal torque requirement about the three axes each wheel's torque capacity must satisfy

$$\dot{H}_{w,mx} \geq T_x/2 \qquad (104)$$

instead of (103).

When the maximum required torque components T_x, T_y, T_z are all equal, Eqs. (99) yield Eq. (81)

$$s\eta_1^* = 1/\sqrt{3} = s\eta_2^*; \quad c\eta_1^* = \sqrt{2}/\sqrt{3} = c\eta_2^*;$$
$$\eta_1^* = 35.26° = \eta_2^* \qquad (105)$$

The two cant angles, therefore, coalesce and indeed they become the same as that for the 4-wheel configurations. The desired maximum torque capacity of the wheel is then found to be

$$\dot{H}_{w,mx} \geq 0.846\, T_x \qquad (106)$$

which is smaller than the torque capacity (82b) or (85b) for 4-wheel configurations for the same torque requirements about the spacecraft axes.

Regarding the power consumption, the Euclidean norm (100) yields

$$\| \underline{\dot{H}}_{ww} \|^2 = 1.5\, T_x^2 \qquad (107)$$

Comparing (107) with (84b) and (87b), we observe that for the same T_x about all three axes, the power consumption of the 6-wheel configuration increases at a smaller rate than that of the 4-wheel configuration. Finally,

$$\sum_{i=1}^{6} | \dot{H}_{wi} | = 2.509\, T_x \qquad (108)$$

which is within the two values (84a) and (87a) for the two 4-wheel configurations.

One-Cant-Angle Configuration

A hexagonal wheel assembly with two different cant angles might be difficult to install in a spacecraft bus; so we now optimize a hexagonal configuration with one cant angle. The pseudo-inverse matrix, Eq. (97), simplifies and Eq. (61) yields the Euclidean norm

$$\| \underline{\dot{H}}_{ww} \|^2 = (T_x^2 + T_z^2) / 3c^2\eta + T_y^2/6s^2\eta \qquad (109)$$

where the subscript 1 of η_1 is dropped because now there is only one cant angle. Minimization of this norm leads to, surprisingly, the condition (72) for the 4-wheel configurations. The minimum value of the norm (109) is

$$\| \underline{\dot{H}}_{ww} \|^2 = \left[T_y + \sqrt{2\,(T_x^2 + T_z^2)} \right]^2 / 6 \qquad (110)$$

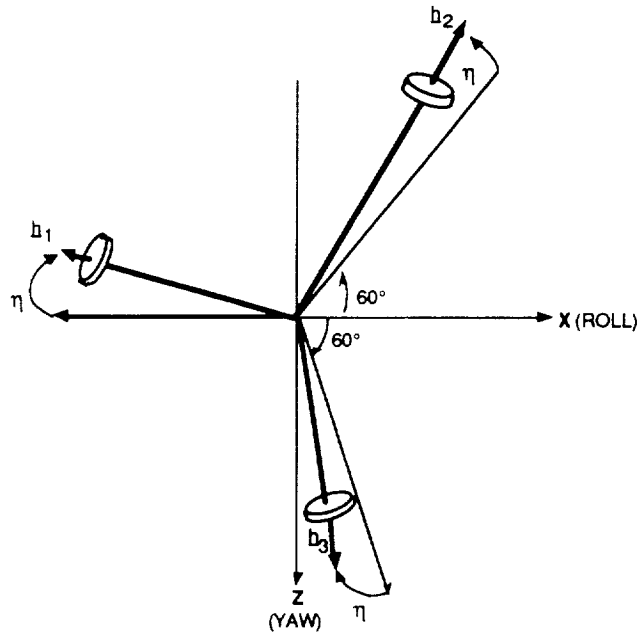

Fig. 17. A Three-Wheel Pyramid Configuration

which is two-thirds of the value in (74) for the 4-wheel configuration. Also, because of the inequality (101), we arrive at

$$\dot{H}_{w,mx} > \left[\sqrt{(T_x^2 + T_z^2)/18} + T_y/6\right] \qquad (111)$$

which is different form (102) but, for equal torque requirement, reduces to (103).

The one-wheel failure analysis, considered above for the four-wheel configurations, becomes unwieldy because of the 5x3 size of the reduced matrix $\underline{C}_{bw}$. Therefore, pertinent results such as wheel torque capacity and power consumption are obtained with the aid of a computer and summarized later in Table 3.

Three-Wheel Pyramid Configuration

When wheel redundancy is not warranted, when for reasons of cost and weight the number of wheels must be bare minimum, and when the torque requirements about the three axes are not necessarily equal, the three-wheel pyramid configuration shown in Fig. 17 might be an ideal choice. For this arrangement, the three wheel angular momentums can be expressed in spacecraft axes as follows:

$$\begin{bmatrix} H_x \\ H_y \\ H_z \end{bmatrix} = \begin{bmatrix} -c\eta & 1/2\ c\eta & 1/2\ c\eta \\ -s\eta & -s\eta & -s\eta \\ 0 & -\sqrt{3}/2\ c\eta & \sqrt{3}/2\ c\eta \end{bmatrix} \begin{bmatrix} H_{w1} \\ H_{w2} \\ H_{w3} \end{bmatrix} \qquad (112)$$

wherein the 3x3 transformation matrix is $\underline{C}_{bw}$. Because now there is no redundancy, the pseudo-inverse matrix $\underline{C}_{bw}^{\dagger}$ becomes the regular inverse matrix $\underline{C}_{bw}^{-1}$. After determining $\underline{C}_{bw}^{-1}$ and substituting that in Eq. (61), the vector $\dot{\underline{H}}_{ww}$ in terms of the required torque components T_x, T_y, T_z turns out to be

$$\dot{\underline{H}}_{ww} = \begin{bmatrix} 2T_x/3c\eta + T_y/3s\eta \\ -T_x/3c\eta + T_y/3s\eta + T_z/3c\eta \\ -T_x/3c\eta + T_y/3s\eta - T_z/3c\eta \end{bmatrix} \qquad (113)$$

For minimization of power consumption, we arrive at the followin Euclidean norm.

$$\| \dot{\underline{H}}_{ww} \|^2 = 2\,(T_x^2 + T_z^2) / 3c^2\eta + T_y^2/3s^2\eta \qquad (114)$$

which is four-thirds of the norm (71) for 4-wheel configurations and six-thirds (twice) of the norm (109) for 6-wheel configuration, implying that if they all begin from zero wheel speed, the 3-wheel configuration will consume greater power in the stated ratio. For example, for equal torque requirements ($T_x = T_y = T_z$), while the minimum value of the 4-wheel norm is 2.25, that of the 3-wheel norm is 3.0, which is, incidentally, the same as that for the three orthogonal wheels one per axis. Moreover, if the cant angle is not set to be the optimum ($\eta \neq \eta^*$), the three-wheel pyramid configuration will use more power than the one-per-axis configuration.Next, the norm (114) yields the same optimum angle as one for the 4- and 6-wheel configurations, Eq. (72). For this optimum angle, the following minimum value of the norm emerges:

$$\| \dot{\underline{H}}_{ww} \|^2_{\ min} = [\ T_y + \sqrt{2(T_x^2 + T_z^2)}\ ]^2/3 \qquad (115)$$

which is twice the value (110) for the 6-wheel configuration and four-thirds of the value (71) for the 4-wheel configuration.

The required torque capacity of the wheels for equal torque requirements about roll, pitch, and yaw axes is found to be

$$\dot{H}_{w,mx} \geq 1.39\ T_x \qquad (116)$$

As a check, note that the norm of $\dot{\underline{H}}_{ww}$ for three-wheel configuration is indeed

$$\| \dot{\underline{H}}_{ww} \|^2 = 3T_x^2 \qquad (117)$$

equal to that for a one-wheel-per-axis configuration; but the power consumption of each wheel would be quite different from that for the one-wheel-per-axis configuration.

Overall Comparison of Six Configurations

When the torque requirements about the roll, pitch, and yaw axes are not the same, the wheels of different torque capacities along different axes might be selected; but from the standpoint of reliability and cost, that is usually not preferred. Perhaps a more attractive choice is a six-wheel configuration with identical wheels, the cant angle selected according to the desired torque ratios. For equal torque requirements, the optimum cant angle is $\eta^* = 35.26°$, and the associated wheel torque capacity for the required torque T_{mx} must be at least 0.846 T_{mx} [Eq. (106)]—greater than 0.5 T_{mx} for the two-wheel-per-axis arrangement. The two power consumption indexes in the case of

no wheel failure shown in the second row of Table 3 restate Eqs. (107) and (108). When the wheel in the roll-pitch plane fails, the torque capacity of the remaining five wheels must be boosted to at least 1.311 T_{mx} to produce the required torque T_{mx} about the spacecraft axes. This result is obtained by failing the wheels 1,2,...,6, one at a time, and then determining the absolute maximum value of the wheel torque in each case for generating T_{mx} torque about each of the three spacecraft axes. The maximum Euclidean norm and the associated absolute sum $\sum_{i=1}^{6} |\dot{H}_{wi}|$ are also shown in Table 3. Comparing the 2-wheel-per-axis and 6-wheel hexagon configurations, we find that for *equal torque requirements*, the latter (hexagon) configuration requires wheels of larger torque capacity and it consumes more power—and therefore not as favored as—the former configuration. However, when the roll, pitch, and yaw torque requirements are not the same, the conclusion will possibly swing in favor of the hexagon configuration.

Although six-wheel configurations provide substantial reliability and three-wheel redundancy, they could be expensive, so four-wheel configurations may be desirable instead, which provide a one-wheel redundancy. Two such configurations—one with pyramid base parallel to roll-yaw axes and the other with the base at 45°—are discussed above. For the purpose of comparison , call these configurations *parallel-* and *45°-*configuration, respectively. Under no-failure case, the 45°-configuration requires wheels of larger torque capacity than the parallel-configuration, but in the event of a one wheel failure, the situation reverses. On the other hand, from the power consumption viewpoint, under no-failure case, the 45°-configuration uses only slightly more power than the parallel-configuration, but the failure of a wheel aggravates this difference. Because the final design is usually based on one-wheel failure performance, we infer that if power is relatively abundant and the wheel torque capacity is at a premium, the 45°-configuration should be selected. On the other hand, if power is expensive and the cost of the wheels depends only weakly on its torque capacity, the parallel configuration will then be a more prudent choice.

When wheel redundancy is not warranted, only three wheels—necessary and sufficient for spacecraft control—can be employed. If the torque and momentum requirements about the three axes are identical, the control engineer may opt for one-wheel-per-axis configuration. But in the case of dissimilar requirements, 3-wheel pyramid, with the cant angle suitable to the desired torque and momentum ratios, might be preferred. Table 3 compares these two 3-wheel configurations for equal torque requirements, and shows that the pyramid configuration requires wheels of 39% bigger torque capacity, although its power consumption may be slightly less than or equal to that of the one-wheel-per-axis configuration.

Fig. 18 sums up the comparison between the power consumption of the six configurations considered in Table 3 for equal torque requirements. In particular, the Euclidean norm of the vector $\dot{H}_{ww}$ versus the cant angle for each configuration for the no-wheel-failure case are shown in the figure. As noted before, the cant angle η^* ($\eta^* = 35.26°$) for minimum power consumption is the same for 3-, 4-, or 6-wheel pyramid configurations.

Concluding Remarks

Among a variety of disturbance torque that act on a space-craft, only solar radiation is considered in the preceding. For clarity, the torque expressions are further specialized by assuming that the vehicle mass center always remains in the pitch-yaw plane. Although this was true for the spacecraft that led to this study, the roll component of the vector from instantaneous vehicle mass center to the geometric center of the array or bus may not be zero for other spacecraft. Also, while solar torque varies at orbit frequency, aerodynamic torque, for

Table 3. Comparison of Six Configurations for Equal Torque Requirements about Roll, Pitch, and Yaw Axes, Based on Minimum Power Consumption

REQUIRED CONTROL TORQUE: $T_{cx} = T_{cy} = T_{cz} = T_{mx}$

CONFIGURATION	OPTIMUM ANGLE η^* (Deg)	NO-FAILURE			WORST 1-WHEEL FAILURE					
					TORQUE			POWER		
		Required Torque Capacity $\dot{H}_{w\cdot mx}/T_{mx}$	Total Power Consumption Rate $\sum_{i=1}^{n_w} \dot{h}_i^2/T_{mx}^2$	Total Power Intercept Due to Nonzero Initial Wheel Speed $\sum_{i=1}^{n_w-1} \lvert\dot{h}_i\rvert/T_{mx}$	Failed Wheel #	Wheel Producing Max. Torque	Required Torque Capacity $\dot{H}_{w\cdot mx}/T_{mx}$	Failed Wheel #	Total Power Consumption Rate $\sum_{i=1}^{n_w} \dot{h}_i^2/T_{mx}^2$	Total Power Intercept Due to Nonzero Initial Wheel Speed $\sum_{i=1}^{n_w-1} \lvert\dot{h}_i\rvert/T_{mx}$
2 Wheel/Axis (n_w=6)		0.5	1.5	3.0	Any One		1.0	Any One	2.0	3
6-Wheel Hexagon (n_w=6)	35.26	0.846	1.5	2.509	#5	#4	1.311	#4	2.933	3.073
4-Wheel Pyramid, Base Edges ∥ to Axes (n_w=4)	35.26	1.045	2.25	2.449	#1 #2	#2 #1	2.091	#1,2	6.62	4.182
4-Wheel Pyramid, Base Edges at 45° to X,Z Axes (n_w=4)	35.26	1.3	2.25	2.598	#3	#1, 2, 4	1.732	#3	9.0	5.196
3-Wheel Pyramid (n_w=3)	35.26	1.39	3.0	2.8	FAILURE DISALLOWED					
3-Orthogonal Wheels (n_w=3)		1	3.0	3.0						

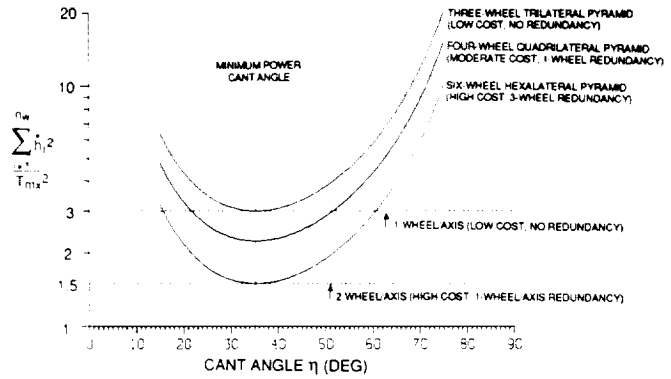

Fig. 18. Reaction wheel configurations trade-offs for equal roll, pitch, and yaw torque requirements

instance, may vary at twice the orbit frequency and a yaw bias torque might arise. For these different circumstances, the torque and momentum expressions have to be derived afresh to size the wheels. Regarding the wheel configurations, besides the two four-wheel configurations considered in the paper, there are two more: 1) NASA's standard four-wheel arrangement of one wheel along each body-axis and the fourth wheel inclined equally to all three axes; and 2) all four wheels canted equally to the pitch axis and each controlling roll and yaw as well, but more inclined to roll-axis than to yaw-axis or the converse depending on the roll and yaw unequal torque requirements. In the first arrangement, the cant angle of the fourth wheel is already determined, only the wheels' torque and momentum capacity need to be sized for one-wheel failure scenario. In contrast, in the second arrangement, two angles must be optimized to minimize power consumption for given torque and momentum requirements: the cant angle η with the roll-yaw plane and the angle γ with the roll axis for all four wheels. For these optimum angles, the torque and momentum capacity of the wheels will be sized according to one-wheel failure condition, as shown in the paper.

References

1. McElvain, R.J , "Effects of Solar Radiation Pressure on Satellite Attitude Control," *ARS Guidance, Control, and Navigation Conference*, Stanford, Ca., August, 1961, also *Guidance and Control—II, Progress in Astronautics and Aeronautics*, Vol. 13, Ed. Langford, R.C. and Mondo, C.J., pp. 543-564
2. Kalweit, C.C., "Optimum Yaw Motion for Satellites with a Nadir-Pointing Payload," *Journal of Guidance, Control, and Dynamics*, Vol. 6, No. 1, January-February, 1983, pp. 47-52
3. Evans, W.J., "Aerodynamic and Radiation Disturbance Torques on Satellites Having Complex Geometry," Chap. 5 in *Torques and Attitude Sensing in Earth Satellites*, Ed. by S.F. Singer, Academic Press, 1964
4. DeBra, D.B., and Cannon, R.H., "Momentum Vector Considerations in Wheel-Jet Satellite Control System Design," *Guidance and Control, Progress in Astronautics and Rocketry*, Vol. 8, Ed. R.E. Roberson and J.S. Farrior, pp. 565-598
5. Hughes, P.C., *Spacecraft Attitude Dynamics*, John Wiley and Sons, 1986
6. Fleming, A.W., and Ramos, A., "Precision Three-Axis Attitude Control Via Skewed Reaction Wheel Momentum Management," AIAA Paper No. 79-1719, Guidance, Naviation, and Control Conference, pp. 177-190